A CONTINUUM MODEL OF PROTRUSION OF PSEUDOPOD IN LEUKOCYTES

CHENG ZHU AND RICHARD SKALAK
Bioengineering Institute, Department of Civil Engineering and Engineering Mechanics, Columbia University, New York, New York 10027

ABSTRACT The morphology of human leukocytes, the biochemistry of actin polymerization, and the theory of continuum mechanics are used to model the pseudopod protrusion process of leukocytes. In the proposed model, the pseudopod is considered as a porous solid of F-actin network, the pores of which are full of aqueous solution. G-actin is considered as a "solute" transported by convection and diffusion in the fluid phase. The pseudopod grows as actin filaments elongate at their barbed ends at the tip of the pseudopod. The driving force of extension is hypothesized as being provided by the actin polymerization. It is assumed that elongation of actin filaments, powered by chemical energy liberated from the polymerization reaction, does mechanical work against opposing pressure on the membrane. This also gives rise to a pressure drop in the fluid phase at the tip of the pseudopod, which is formulated by an equation relating the work done by actin polymerization to the local state of pressure. The pressure gradient along the pseudopod drives the fluid filtration through the porous pseudopod according to Darcy's Law, which in turn brings more actin monomers to the growing tip. The main cell body serves as a reservoir of G-actin. A modified first-order equation is used to describe the kinetics of polymerization. The rate of pseudopod growth is modulated by regulatory proteins. A one-dimensional moving boundary problem based on the proposed mechanism has been constructed and approximate solutions have been obtained. Comparison of the solutions with experimental data shows that the model is compatible with available observations. The model is also applicable to growth of other cellular systems such as elongation of acrosomal process in sperm cells.

I. INTRODUCTION

The ability of leukocytes to perform active movements is vital to their functions in defensive mechanisms of the body against diseases, in tissue inflammation, in wound healing, and in other physiological and pathological processes. In phagocytosis, the cell projects enveloping pseudopods around the circumference of foreign particles such as bacteria and aging or fragmented cells, and these pseudopods fuse with one another to complete engulfment (Orenstein and Shelton, 1977). In locomotion in a chemotactic gradient or migration across a capillary wall into interstitium, the cell translocates in an amoeboid-like movement. The cell, when adhering to a substrate, say the endothelium of blood vessel wall, flattens itself and then extends part of its cytoplasm and membrane beyond the original perimeter of the cell to form a projection in the direction of locomotion. This newborn motile appendage (pseudopod) attaches to the substrate and then exerts a traction on the rest of the cell. The posterior attachment on the tail of the cell breaks down in a tug-of-war and the cell is thus pulled ahead. This process repeats in cycles and thereby displaces the cell on the substrate (Schmid-Schönbein, 1987). These active movements involve formation of pseudopods, which is a fundamental event in leukocyte locomotion (Tranquillo and Lauffenburger, 1987; Tranquillo et al., 1988).

A leukocyte can also form pseudopods spontaneously when freely suspended in plasma or autologous Ringer's solution (Schmid-Schönbein et al., 1982). Pseudopod formation is therefore itself an active motile process because the driving force and energy required to produce motion are derived internally from the cell. In the case of spontaneous pseudopod formation of leukocytes suspended in isotonic solution, no external forces other than a hydrostatic pressure and the gravity are acting on the cell. A central hypothesis of the present work is that some of the chemical energy liberated during actin polymerization may be the source of mechanical work done in extending the pseudopod.

The gross rheological properties of leukocytes have been investigated using the micropipette aspiration technique (Schmid-Schönbein et al., 1981; Sung et al., 1982; Chien et al., 1982, 1984). A recent work shows that the overall mechanical behavior of a passive neutrophil without pseudopods can be modeled by an incompressible Maxwell fluid interior enclosed by an elastic shell (Dong et al., 1988). For neutrophils in active state with pseudopods, the main bodies of the cells behave similarly to passive cells whereas the pseudopods are elastic and much stiffer than the main cell bodies (Schmid-Schönbein et al., 1982).

The difference in rheological properties between different regions in leukocytes reflects the fact that the composition and ultrastructure of the pseudopod are quite

different from those of the main cell body. When observed by transmission electron microscopy (EM) (Fig. 1 *a*), the main cell body is seen to contain mostly cytoplasm (over 60% for neutrophils; Schmid-Schönbein, 1987) and formed elements such as the nucleus and various granules, whereas the pseudopod is seen to contain very few, if any, cell organelles at least in the early stages of formation. The pseudopod in EM shows a uniform and isotropic fine fibrillar structure, which is identified as actin microfilaments cross-liked by actin-binding proteins (e.g., Stossel, 1988). Actin filaments in the network in many cell types are known to have a uniform polarity such that their fast growing, or barbed, ends are distal to the tip of the pseudopod attaching to the plasma membrane whereas the slowly growing, or pointed, ends are at the base of the pseudopod attaching to the main cell body (Hartwig and Shevlin, 1986; Pryzwansky et al., 1983). The properties of gels, such as an actin network, have been recently estimated by a statistical mechanics theory (Nossal, 1988) and are shown to be quite stiff.

Besides formed elements and cytoskeletal matrix, the majority of the cell volume is occupied by aqueous solution of water, physiological ions, and macromolecular proteins, most notably G-actin. It has been estimated that the monomeric actin concentration within leukocytes is of the order of 7 mg/ml (~167 μM, see Section IV), which is three orders of magnitude higher than the critical concentration of G-actin required to initiate polymerization into F-actin under normal physiological ionic strength in vitro (~0.1 μM) (Carson et al., 1986). This high actin concentration (compared with the critical concentration) is kept unpolymerized by formation of a tight complex, called profilactin, in 1:1 ratio with profilin (which is a regulatory protein with a molecular weight of 15,220), which inhibits the polymerization (e.g., Korn, 1982; Pollard and Cooper, 1986). The unpolymerized actin is freely diffusible within the main cell body as well as through the pores in the pseudopods. This is because the framework of the fibrous actin network in pseudopods is far from compact but is mostly composed of pores. Estimation of the pore size ranges from 20 nm (Luby-Phelps et al., 1986) to 100 nm (Hartwig and Shevlin, 1986), which is large enough for profilactin and other macromolecules to percolate through, and yet small enough to exclude the organelles. (Profilactin has a Stokes' radius of 2.9 nm [Lassing and Lindberg, 1985].) The diffusion coefficent of G-actin in aqueous solution has been measured to be ~5–8 $\times$ 10^{-7} cm^2/s (Mihashi, 1964; Lanni et al., 1981; Tait and Freiden, 1982; Montague et al., 1983; Lanni and Ware, 1984). Measurements of the diffusion coefficient of G-actin in the cytoplasm of living cells, however, resulted in diverse and conflicting data. Wang and co-workers (1982) found that the diffusion coefficient of G-actin in living amebas had the same order of magnitude as, but a few-fold smaller than, that in buffer solution. On the other hand, Kreis and colleagues (1982) obtained a G-actin diffusion coefficient in living embryonic chicken gizzard cells two orders of magnitude smaller (~10^{-9} cm^2/s) than that in aqueous solution. The diffusion coefficient of G-actin in living fibroblasts measured by Felder (1984) lay in-between with a value of ~10^{-8} cm^2/s.

The large excess of unpolymerized actin above critical concentration and its ability to diffuse within leukocytes, as in many other nonmuscle cells, ensures the availability of actin subunits when conditions are favorable for polymerization at specific sites, as at the tip of the pseudopod during the protrusion process. The initiation, rate, and extent of actin polymerization are regulated by various proteins and ionic environments. For example, interaction of profilaction with PIP_2, a phospholipid associated with the plasma membrane, causes rapid and efficient dissociation of the profilin–actin complex. The liberated actin is then available for polymerization in appropriate conditions (Lassing and Lindberg, 1985). In addition to actin monomer binding proteins such as profilin, actin polymerization is also regulated by actin filament capping proteins, such as gelsolin, which block filament barbed ends and inhibit the addition of actin monomers to them. Gelsolin and other capping proteins are found to localize within the cell cortex, especially near the plasma membrane to which the F-actin barbed ends attach (Yin et al., 1981; Cooper et al., 1984). The capping proteins are in turn modulated by polyphosphoinositides and ionic conditions such as Ca^{2+} concentration.

The fact that the pseudopod contains more actin filaments than the main cell body suggests that actin is polymerized during pseudopod extension and is depolymerized during pseudopod retraction. There are several experimental observations which suggest that actin polymerization occurs at the tip of the pseudopod and that depolymerization occurs at the base of the pseudopod. Pseudopods have been observed to branch like a tree during the course of their formation. Daughter pseudopods extend in length as the tree grows. In another observation, a filipod of fibroblast bent sharply and grew upward from a point of bend (which remained fixed), i.e., the distance between the bend point and the cell body remained constant while that from the bend point to the tip of the filipod increased. When a fine quartz fiber (fishpole) was used to probe the stiffness of this microspike, it was found to be quite stiff and largely elastic (Felder, 1984). It is argued that if the growth occurred at the base, the rigid F-actin matrix inserted at the base would then have to be divided into parts at branch points and bend sharply at the bend points, which is not likely to occur in rigid networks.

In another experiment, fluorescently labeled actin was microinjected into living fibroblasts and was incorporated into stable microfilament networks within the leading lamella (which are similar to pseudopods). A small spot near the edge of the leading lamella was photobleached by

a laser microbeam which destroyed the emission of the fluorescently labeled actin in the network within the spot. The movement of the spot was then recorded and correlated with the motion of the lamellapod. The observations showed that the bleached spot remained stationary while the lamellapod grew. This implied that the actin filament network did not move out with the extending lamellapod (Felder, 1984). Wang (1985) studied the movement of the bleached spot in steady lamellipodium. The spot was found to move through an unbleached region backward toward the center of the cell. Both experiments indicate that incorporation of actin subunits occurs predominantly at the membrane-associated, barbed ends of actin filaments.

The notion of growth at the tip has also been supported by observations made on elongation of other cellular processes containing actin filament matrix. Tilney and co-workers observed that elongation of acrosomal processes in *Limulus* and *Thyone* sperms occurred at the growing tip (Tilney et al., 1981; Tilney and Inoué, 1982). Detmers and colleagues found that cytochalasin D, a drug which binds to actin filament barbed ends and thereby prevents F-actin from elongation, inhibited the growth of fertitization tubule in *Chlamydomonas reinhardti* (Detmers et al., 1983).

The assumption of growth at the tip is consistent with the facts that the growth of actin filaments is faster, and is generally regulated, at the barbed ends, and that the barbed ends as well as capping proteins generally attach to the plasma membrane. If growth were to occur at the base of the pseudopod, actin polymerization would have to take place at the pointed ends of microfilaments, which is a less favorable process.

An essential concept in the present paper is that the polymerization of actin may be the source of both energy and force of the pseudopod formation. Hill (1981) has discussed the possible motion resulting from lengthening or shortening of actin microfilaments. It is shown that the notion of actin polymerization doing mechanical work against an opposing force is compatible with the laws of thermodynamics (also see Hill and Kirschner, 1982). The basic idea is that actin filaments with their barbed ends attaching to the plasma membrane can elongate by adding G-actin to the barbed ends, thereby pushing the deformable membrane outward, against a compressing force that resists the growth. The driving energy is the change of chemical potential of actin from monomeric to polymeric states and is probably dependent on the accompanying hydrolysis of ATP.

In this work, a continuum model for pseudopod protrusion in leukocytes based on actin polymerization is proposed. The essential elements of the model are:

(*a*) The pseudopod is assumed to be a porous medium of actin gel. The network of actin filaments forms a stiff framework which provides the rigidity of the pseudopod. The motion of aqueous solution in the pores of the actin matrix is assumed to be driven by a pressure gradient according to Darcy's law.

(*b*) Monomeric actin is considered as slowly diffusing solute dispersed within the fluid phase, transported by convection and diffusion, and is converted to actin filaments at the sites of polymerization.

(*c*) Elongation of actin filament, powered by chemical free energy liberated form polymerization reaction, does mechanical work by pushing the cell membrane outwards against an opposing pressure. The membrane motion creates a pressure drop at the tip of the growing pseudopod inside the cell which provides the driving force for the fluid flow.

(*d*) The pseudopod extends as a result of actin polymerization at the tip of the pseudopod. The building blocks are transported from the main cell body through the gel to the growing tip.

(*e*) The actin polymerization is governed by a simple reaction kinetics equation. The rate of growth is modulated by regulatory proteins.

The present model has some similarities to, but also essential differences from, other models of cell motility in the literature. Oster and co-workers have proposed a model for the elongation of acrosomal process in *Thyone* sperms and for the spreading of lamellipod in amoeboid cells based on an osmotic swelling driving mechanism (Oster et al., 1982; Oster, 1984; Oster and Odell, 1984; Oster and Perelson, 1985, 1987). Dembo and colleagues have developed an "interpenetrating reactive flow" model for surface protrusion and other motion in amoeboid cells based on contraction due to actin–myosin interaction (Dembo et al., 1984; Dembo, 1986; Dembo and Harlow, 1986). Schmid-Schönbein and Skalak (1984) proposed a model for pseudopod formation in leukocytes based on contraction due to polymerization of actin at the base of the pseudopod with preferred orientation. Tilney and Kallenbach (1979) proposed, and Perelson and Coutsias (1986) later improved, a moving boundary model for elongation of the acrosomal process in *Thyone* sperms based on actin polymerization. None of the above models directly assume work done by actin polymerization as the driving mechanism, although several clearly call for actin polymerization and growth at the tip.

In the next section the governing equations, and boundary and initial conditions for a one-dimensional system will be derived based on the above scheme, which will lead to a convection/diffusion-reaction moving boundary problem. In Section III, the moving boundary value problem will be solved using approximate methods. In Section IV, relevance of our solutions to biological problems will be evaluated by comparing the theoretical results with experimental data. In the last section, the one-dimensional formulation will be generalized to three-dimensional cases and the validity of various simplifying assumptions made during the course of modeling will be discussed.

II. DERIVATION OF THE GOVERNING EQUATIONS

In this section a moving boundary model for pseudopod protrusion in leukocytes is developed based on the experimental observations outlined in the Introduction. For the sake of simplicity, the governing equations and boundary conditions are derived for a one-dimensional case. The generalization to three dimensions will be derived in Section V.

Geometry and Field Variables

A leukocyte with a pseudopod is considered to consist of two different regions: the main cell body and the pseudopod (see Fig. 1 *b*). The main cell body contains all cell organelles and is considered to be a viscoelastic fluid. Since the main cell body is not our concern in this approach, it is regarded as a reservoir which provides appropriate boundary conditions for the dynamics of the pseudopod. The pseudopod consists of two distinct phases: a solid framework of actin microfilaments and a fluid suspension which fills the pores of the network. The pseudopod is therefore assumed to be a porous medium. The fluid volume fraction is denoted by ϕ (which is also the porosity of the porous medium), so the solid volume fraction is $(1 - \phi)$. In the present analysis, ϕ is taken to be constant. The fluid phase in a pseudopod is a complex aqueous solution of macromolecular proteins and small ions. Such a fluid is modeled by recognizing G-actin as a slowly diffusing "solute" and lumping water and other rapidly diffusing particles into a homogeneous "solvent." The concentration of the solute, c, is defined as the number of G-actin molecules per unit fluid volume.

In the one-dimensional formulation, the pseudopod is modeled as a cylinder or sheet of constant cross-sectional area (Fig. 1 *b*). A coordinate system is introduced with the x axis along the long axis of the pseudopod. The origin of x is at the base of the pseudopod, and $x = s(t)$ is the position of the growing tip (t denotes time). The physical quantities of interest are the location of the tip (s as a function of t), the concentration distribution of G-actin (c as a function of x and t), the mean velocity of the fluid over the pore area (v as a function of x and t), and the pore hydrostatic pressure (p as a function of x and t). Specifying the dependence of c, v, and p upon x and t alone but not other spatial coordinates implies that the model deals with the average of these quantities but not with their local variations over a cross-section.

The differential equations and boundary and initial conditions which s, c, v, and p satisfy are next derived according to the conservation laws of continuum mechanics.

Conservation of Mass

The fluid suspension is considered to be incompressible. Since the porosity ϕ is assumed to be constant, the continuity equation for the fluid phase becomes

$$\frac{\partial v}{\partial x} = 0 \quad \text{in} \quad 0 < x < s. \tag{1}$$

Since it is assumed that no polymerization occurs inside the shaft of the pseudopod, the conservation of actin monomers within the pseudopod leads to

$$\frac{\partial}{\partial t}\phi c = \frac{\partial}{\partial x}\phi'\left(-vc + D\frac{\partial c}{\partial x}\right), \tag{2'}$$

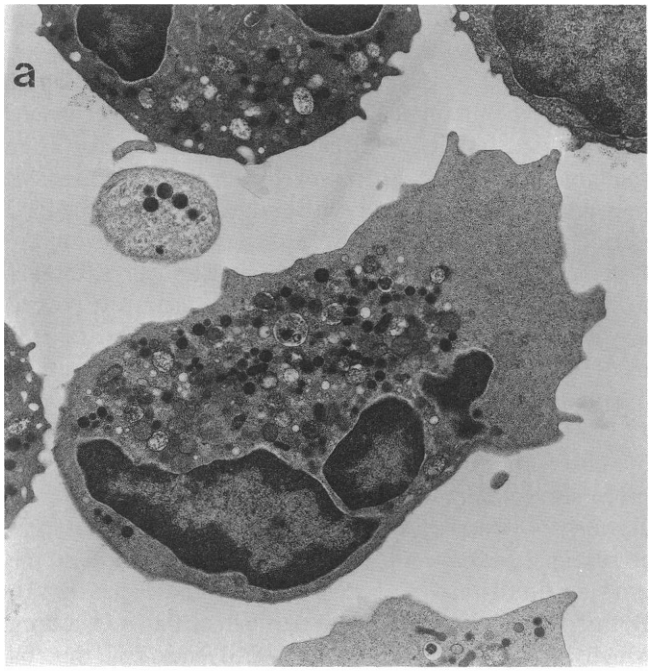

FIGURE 1 (*a*) Transmission electron micrograph of a human neutrophil with a pseudopod (provided by G. W. Schmid-Schönbein). The main cell body can be seen to contain nucleus and granules. The pseudopod consists of a uniform structure. (*b*) Schematic illustration of *a*. The main cell body is represented by viscoelastic sphere. The pseudopod is represented by a cylinder or sheet with constant cross-sectional area. The origin of the coordinate system is at the base of the pseudopod, and $x = s$ is the position of the growing tip. Illustrated also in the figure are actin filaments with their barbed ends attached to the growing tip, polymerization front, and the reaction chamber at the tip (see text).

where D is the diffusion coefficient (assumed to be constant), ϕ' is the fraction of a cross-sectional area of the pseudopod occupied by the fluid. For an isotropic porous medium, $\phi' = \phi$ so that ϕ and ϕ' cancel from both sides of the equation. Using Eq. 1, Eq. 2' can be written in the form of the usual convection-diffusion equation:

$$\frac{\partial c}{\partial t} + v\frac{\partial c}{\partial x} = D\frac{\partial^2 c}{\partial x^2} \quad \text{in} \quad 0 < x < s. \tag{2}$$

At the tip of the pseudopod where polymerization takes place, actin molecules undergo change in state from monomeric to polymeric. The mass conservation law of actin molecules at the tip must take this reaction into account. The rate of monomeric actin supply to the growing front via convection and diffusion is $\phi'(vc - D\partial c/\partial x)$ (per unit cross-sectional area). Part of the actin monomers polymerize into the filament network and form new porous media at the tip. The rest of the actin monomers are dispersed as solute inside the newborn pores. Let n be the number of filament ends per unit tip surface area and let l be the length by which a filament extends due to the addition of one monomer to the filament. The velocity of the pseudopod growth is ds/dt, which is also proportional to the average rate of actin filament elongation. Hence the amount of G-actin that is polymerized is $(n/l)ds/dt$, per unit cross-sectional area per unit time. The volumetric rate of pore generation is $\phi(ds/dt)$ (per unit cross-sectional area). The amount of G-actin dispersed inside the newborn pores is $\phi c(ds/dt)$ (per unit cross-sectional area per unit time). The conservation of actin molecules thus leads to

$$\phi'\left(vc - D\frac{\partial c}{\partial x}\right) = \left(\frac{n}{l} + \phi c\right)\frac{ds}{dt} \quad \text{at} \quad x = s. \tag{3}$$

Note that (n/l) is the number of actin protomers per unit volume in the filament network. In this one-dimensional (1-D) model all filament barbed ends are assumed to be lined up at the tip position $x = s$ and all filaments are assumed to extend in the positive x direction. These constraints will be relaxed in the three-dimensional (3-D) formulation.

Equation of Fluid Motion

Since the solid matrix is treated as rigid porous medium through which the fluid filters, it is assumed that within the pseudopod the fluid flow obeys Darcy's law. Darcy's law does not deal with the detailed interactions between the two phases but accounts for the average resistance of the solid to the fluid by a permeability coefficient, K. This is a valid approximation to the average biphasic field theory provided Reynolds' number of the flow is much less than one (for example, see Scheidegger, 1974). In the present 1-D case, Darcy's law reduces to

$$v = -\frac{K}{\phi\mu}\frac{\partial p}{\partial x} \quad \text{in} \quad 0 < x < s, \tag{4}$$

where μ is the fluid viscosity.

Conservation of Energy

The first law of thermodynamics applied to a small control volume (reaction chamber, see Fig. 1 *b*) at the tip of the pseudopod (including the membrane portion), where actin polymerization takes place can be written as

$$\Delta\mu\frac{n}{l}\frac{ds}{dt} + \alpha\left(\frac{ds}{dt}\right)^2 + q = (p_e - p)\frac{ds}{dt} + \frac{dU}{dt}. \tag{5}$$

In Eq. 5, the first term is the rate of chemical energy liberation of actin polymerization (per unit area of tip surface), in which $\Delta\mu$ is the chemical energy release due to the transition of state of one molecule from G-ATP–actin to F-ADP–actin. The second term represents dissipation due to viscous losses, in which α is a dissipative coefficient. q in Eq. 5 stands for rate of heat transfer, if any, to the reaction chamber from the surroundings. The first term on the right-hand side of Eq. 5 is the rate of work done (per unit area of tip surface) by the pore hydrostatic pressure, p, on the inner side and the external pressure, p_e, on the outer side of the membrane at the growing tip. The last term of Eq. 5 represents the rate of change of internal and kinetic energies of the reaction chamber (per unit area of tip surface), U, including the contribution due to diffusive and convective transport. The work done by membrane tension has not been included in Eq. 5 since the membrane tension is negligibly small until the membrane foldings are stretched out (Schmid-Schönbein et al., 1981) and in this 1-D model the membrane tension is normal to the direction of the motion.

It is assumed that some of the chemical energy liberated from actin polymerization is used to do mechanical work and the remainder is converted into internal energy and/or dissipated into heat. The efficiency of energy transduction from chemical potential to mechanical work is

$$\eta = \frac{(p_e - p)(ds/dt)}{\Delta\mu(n/l)(ds/dt)} = \frac{\text{mechanical work done}}{\text{chemical energy release}}. \tag{6}$$

The efficiency η must be less than one and greater than zero. Its value depends upon the nature of polymerization and physicochemical conditions under which the reaction takes place, but it is taken to be a constant at the present time. With η defined by Eq. 6, Eq. 5 can be split into two sub-equations:

$$p = p_e - \eta\Delta\mu\frac{n}{l} \tag{7}$$

and

$$(1 - \eta)\Delta\mu\frac{n}{l}\frac{ds}{dt} + \alpha\left(\frac{ds}{dt}\right)^2 + q = \frac{dU}{dt}. \tag{8}$$

Eq. 7 relates the chemical energy liberation of actin polymerization to the local pressure at the inner side of the membrane at the tip of the pseudopod. Note that $\eta\Delta\mu(n/l)$ in Eq. 7 is equivalent to an active normal stress acting on

the membrane applied by the filaments due to the actin polymerization. It pushes the membrane outwards and thereby generates a pressure drop suction in the fluid phase at the tip. This results in a pressure gradient along the shaft of the pseudopod which drives the fluid flow through the porous medium.

Polymerization Kinetics

Pollard and Mooseker (1981) have described their experimental data of elongation of actin filaments in a macroscopic reaction vessel by the following equation

$$\frac{1}{l}\frac{dL}{dt} = k_+c - k_-, \tag{9}$$

in which dL/dt is the rate of elongation of an individual actin filament measured under the microscope; k_+ and k_- are, respectively, association and dissociation rate constants. The equation used by Pollard and Mooseker (1981) was $dL/dt = k_+c - k_-$, but their measured rate constants have been adopted to Eq. 9. Note that $(1/l)(dL/dt)$ is the number of actin monomers added to (or released from) an individual filament per unit time. If both sides of Eq. 9 are multiplied by C, the number density (per unit volume) of F-actin ends reacting with G-actin, the left-hand side, $(C/l)(dL/dt)$, becomes the rate of actin monomers polymerized into (or depolymerized from) actin filaments per unit volume. This should be equal to the reduction (or insertion) of number of actin monomers per unit volume per unit time due to polymerization, i.e., $(C/l)(dL/dt) = -(dc/dt)$. Thus

$$\frac{dc}{dt} = -C(k_+c - k_-). \tag{10}$$

Eq. 10 has been theoretically derived by Wegner and Savko (1982) for a simple nucleation elongation process (also see Frieden, 1985). This equation is to be adopted to apply to elongation reaction localized at the growing tip of the pseudopod.

In the derivation of Eq. 3, the growth is assumed to occur at a surface of infinitesimal thickness. However, in order to deal with the polymerization kinetics, one needs to think of a reaction chamber of small but finite thickness, h, at the tip of the pseudopod (see Fig. 1 *b*). (Note that the reaction chamber concept has also been employed in the consideration of conservation of energy at the tip.) This is because the assumption that all filament ends line up at a surface is valid only in an average sense. Due to the interaction of capping proteins (see below), individual filaments take turns to elongate. A reasonable estimate for h may be the average lateral distance between parallel filaments, i.e., the pore size of the porous medium. Such a reaction chamber, however, differs from the one used in vitro experiments in several aspects. Firstly, it is moving along with the growing tip with the velocity ds/dt. Therefore the time derivative of Eq. 10 should be replaced by material derivative, i.e., $dc/dt = \partial c/\partial t + (ds/dt)(\partial c/\partial x)$. Second, this reaction chamber is an open system rather than a closed container. In addition to polymerization, there is a contribution to the rate of concentration change within the pool from diffusion across one side of the chamber wall, $-D(\phi/h)(\partial c/\partial x)$, but not the other side because it is blocked by the cell membrane. Inclusion of all these effects suggests that the reaction kinetics Eq. 10 should be modified to

$$\frac{\partial c}{\partial t} + \frac{ds}{dt}\frac{\partial c}{\partial x} = -C(k_+c - k_-) - D\frac{\phi}{h}\frac{\partial c}{\partial x} \quad \text{at} \quad x = s. \tag{11}$$

Eq. 11 is to be evaluated at $x = s$ because the thickness of the reaction chamber, h, is much smaller than the length of the pseudopod, s.

Regulation by Capping Proteins

A question in regard to Eq. 11 is how to interpret C, the concentration of F-actin participating in polymerization at the growing tip of the pseudopod. The concentration of total filament ends is (n/h) because there are on average n filament ends per unit cross-sectional area in the reaction chamber of thickness h. However, those filament ends which are blocked by capping protein (say gelsolin) are inhibited from polymerization. C should therefore be interpreted as the concentration of free ends of F-actin because only free ends can react with G-actin. To relate the concentration of free ends to that of total ends, the following capping reaction is considered:

$$\text{capped end} \rightleftharpoons \text{free end} + \text{free gelsolin}, \tag{12}$$

the equilibrium state of which is described by

$$\frac{[\text{capped ends}]}{[\text{free ends}][\text{free gelsolin}]} = K_d, \tag{13}$$

in which square brackets denote concentrations (number density per unit volume) and K_d is the equilibrium constant (Walsh et al., 1984; Wanger and Wegner, 1985). Since

$$[\text{free ends}] + [\text{capped ends}] = [\text{total ends}],$$

and

$$[\text{free gelsolin}] + [\text{bound gelsolin}] = [\text{total gelsolin}]$$

and from stoichiometry

$$[\text{capped ends}] = [\text{bound gelsolin}],$$

the concentration of free ends, C, can be found from Eqs. 12 and 13 and expressed as

$$C = \frac{1}{2}\left(\frac{n}{h} - c_p - \frac{1}{K_d}\right) + \left[\frac{1}{4}\left(\frac{n}{h} - c_p - \frac{1}{K_d}\right)^2 + \frac{n}{h}\frac{1}{K_d}\right]^{1/2}, \tag{14}$$

where c_p is the concentration of total gelsolin at the growing tip. c_p is assumed to be a constant because gelsolin,

like other capping proteins, seems to be localized at the cell membrane (Yin et al., 1981; Cooper et al., 1984; Pollard and Cooper, 1986). K_d is sensitive to secondary messengers such as calcium ion and thereby allows regulation of free end concentration and in turn, the rate of actin polymerization.

It is worth noting that instead of free ends, the total number of filament growing points is used in the equation of conservation of actin molecules at the tip [(n/l) in Eq. 3]. This is because the equilibrium state of the capping reaction (Eq. 12) is understood to be dynamic. Although the fraction of free ends is kept constant, the capping and dissociation continuously proceed with the equal rate in opposite directions. Thus capping takes turns among all filament ends. Every end has the same average frequency of being capped or free. This concept is best expressed by the following equation:

$$\frac{ds}{dt} = \frac{C}{(n/h)} \frac{dL}{dt}, \tag{15}$$

which is obtained by comparing Eq. 3 with Eq. 11 and using Eq. 9. It states that the average rate of extension of all filaments is a fraction of the rate of elongation of an individual free filament. The numerical value of this fraction is equal to the fraction of free ends. Since the concentration of free ends C depends on actin filament capping reaction (Eq. 12) and the concentration of G-actin c depends on actin monomer binding reaction (see Eq. 65 in Section V), Eqs. 11, 12, and 65 imply that the rate of pseudopod growth is modulated by regulatory proteins.

Boundary and Initial Conditions

Eqs. 3, 7, and 11 are boundary conditions at the moving tip ($x = s$). In addition the following boundary conditions are assumed at the fixed base ($x = 0$):

$$p = p_i \quad \text{at} \quad x = 0 \tag{16}$$

and

$$c = c_i \quad \text{at} \quad x = 0, \tag{17}$$

where p_i and c_i are constant values in the main body of the cell. The initial conditions at $t = 0$ when the pseudopod growth starts are

$$c = c_i \quad \text{at} \quad t = 0 \tag{18}$$

and

$$s = 0 \quad \text{at} \quad t = 0. \tag{19}$$

Spatial Dependencies of Fluid Velocity and Pressure

Eqs. 1–4, 7, 11, 16–19 form a well-posed set of equations with appropriate boundary and initial conditions which completely determine four unknown functions v, p, c, and s. The boundary conditions of Eqs. 16 and 17 at $x = 0$ connect the dynamics of the pseudopod with parameters of the main cell body, which serves as a reservoir.

The spatial dependencies of v and p can readily be found form Eqs. 1, 4, 7, and 16. The results are that the velocity is independent of x and the pressure is linear in x:

$$v = \frac{K}{\phi\mu s}\left(p_i - p_e + \eta\Delta\mu \frac{n}{l}\right) \quad \text{in} \quad 0 \le x \le s, \tag{20}$$

$$p = p_i - \left(p_i - p_e + \eta\Delta\mu \frac{n}{l}\right)\frac{x}{s} \quad \text{in} \quad 0 \le x \le s. \tag{21}$$

The temporal dependencies of v and p are not known until the location of the tip, s as a function of t, is determined.

Nondimensionalization

The formulation derived above yields a set of coupled, nonlinear equations the solutions of which depend upon sixteen parameters, namely, ϕ, μ, K, D, p_i, p_e, η, $\Delta\mu$, n, l, h, K_d, c_p, c_i, k_+, and k_-. To facilitate the analysis of this formidable moving boundary problem, the equations are first written in dimensionless form.

The combination $(Ck_+)^{-1}$ possesses the dimension of time and is the characteristic relaxation time of polymerization reaction. The dimensionless time variable $\bar{t}$ is introduced by

$$\bar{t} = (Ck_+)t. \tag{22}$$

The length scale is chosen as $(D/Ck_+)^{1/2}$, which is the characteristic length of diffusion of G-actin in the time scale of actin polymerization. The dimensionless length variable, $\bar{x}$, and pseudopod length, $\bar{s}$, are defined, respectively, as

$$\bar{x} = \left(\frac{Ck_+}{D}\right)^{1/2} x \quad \text{and} \quad \bar{s}(\bar{t}) = \left(\frac{Ck_+}{D}\right)^{1/2} s(t). \tag{23}$$

The dimensionless concentration variable, $\bar{c}$, is constructed as

$$\bar{c}(\bar{x}, \bar{t}) = \frac{c(x, t) - k_-/k_+}{c_i - k_-/k_+}. \tag{24}$$

A convection parameter is defined as the permeability multiplied by the pressure difference across the shaft of the pseudopod and divided by the viscosity and the fracitonal volume of the fluid, i.e., $(K/\phi\mu)(p_i - p_e + \eta\Delta\mu n/l)$. From Eq. 20, this parameter is equal to vs and has the same dimension, $(\text{length})^2(\text{time})^{-1}$, as the diffusion coefficient, D. The ratio of the two defines a dimensionless parameter, the mass transfer Peclet number, as

$$Pe = \frac{vs}{D} = \frac{K(p_i - p_e + \eta\Delta\mu n/l)}{\phi\mu D}, \tag{25}$$

which is a measure of the relative importance of convection and diffusion in the transport of G-actin within the pseudo-

pod. The mass transfer Biot number, Bi, is defined by

$$Bi = \frac{h}{\phi}\left(\frac{Ck_+}{D}\right)^{1/2}, \tag{26}$$

which is the dimensionless thickness of the reaction chamber. Two dimensionless concentration parameters are defined, respectively, by

$$C_1 = \frac{k_-/k_+}{c_i - k_-/k_+} \quad \text{and} \quad C_2 = \frac{n/(\phi l) + k_-/k_+}{c_i - k_-/k_+}, \tag{27}$$

where C_1 is the dimensionless critical concentration and C_2 is the sum of dimensionless concentration of filament growing points and dimensionless critial concentration. $St = 1/C_2$ is the mass transfer Stefan number. C_2 is used here instead of Stefen number for the sake of simplicity of formulas.

Substituting Eqs. 20 and 22–27 into Eqs. 2, 3, 11, and 17–19 yields the following system of nondimensionalized equations:

$$\begin{cases} \dfrac{\partial \bar{c}}{\partial \bar{t}} + \dfrac{Pe}{\bar{s}}\dfrac{\partial \bar{c}}{\partial \bar{x}} = \dfrac{\partial^2 \bar{c}}{\partial \bar{x}^2} & \text{in} \quad 0 < \bar{x} < \bar{s}, \bar{t} > 0, \\ -\dfrac{\partial \bar{c}}{\partial \bar{x}} + \dfrac{Pe}{\bar{s}}(\bar{c} + C_1) = (\bar{c} + C_2)\dfrac{d\bar{s}}{d\bar{t}} & \text{at} \quad \bar{x} = \bar{s}, \bar{t} > 0, \\ \dfrac{\partial \bar{c}}{\partial \bar{t}} + \left(\dfrac{d\bar{s}}{d\bar{t}} + \dfrac{1}{Bi}\right)\dfrac{\partial \bar{c}}{\partial \bar{x}} = -\bar{c} & \text{at} \quad \bar{x} = \bar{s}, \bar{t} > 0, \\ \bar{c} = 1 & \text{at} \quad \bar{x} = 0, \bar{t} \geq 0, \\ \bar{c} = 1 & \text{at} \quad \bar{t} = 0, \\ \bar{s} = 0 & \text{at} \quad \bar{t} = 0. \end{cases} \tag{28}$$

After nondimensionalization, the system of Eqs. 28 looks simpler and is easier to analyze. Only four dimensionless parameters remain, namely, Pe, Bi, C_1, and C_2. Thus the influence of the sixteen dimensional parameters on the behavior of the solutions of the system is incorporated into the four dimensionless parameters, Pe, Bi, C_1, and C_2.

III. APPROXIMATE SOLUTIONS TO THE MOVING BOUNDARY PROBLEM

No closed form solution to the convection-diffusion reaction moving boundary problem of Eqs. 28 is readily obtainable because of the nonlinear nature of the system. However, there are two cases, namely, (*a*) large Peclet number $Pe \gg 1$ and (*b*) long time $\bar{t} \gg 1$, for which approximate analytical solutions can be derived.

Perturbation Solution for Convection-dominated Transport

When the mass transfer Peclet number, Pe, is much greater than unity, convection dominates over diffusion in G-actin transport from the base to the tip of the pseudopod. In this case, Eqs. 28 can be solved approximately by using a singular perturbation method. Perturbation theory seeks a solution in the form of a power series of a small parameter. Because the series is asymptotic, a few leading terms in the series may give a good approximation when the perturbation parameter is sufficiently small (e.g., Nayfeh, 1981).

When $Pe \gg 1$, the G-actin concentration profile will develop a boundary layer of thickness of $Pe^{-1/2}$ at the tip of the pseudopod. Away from the boundary layer, G-actin concentration has a uniform distribution $\bar{c} \sim 1$ ($Pe \to \infty$). This is the "outer solution" which is asymptotic to the true solution in the "outer region" where the diffusion term, $\partial^2\bar{c}/\partial\bar{x}^2$, is small compared with the convection term $(Pe/\bar{s})(\partial\bar{c}/\partial\bar{x})$ (cf. the first equation of Eqs. 28). However, the outer solution cannot satisfy the boundary conditions at $\bar{x} = \bar{s}$. To meet these boundary conditions (the second and third equations of Eqs. 28) the true solution drops down very rapidly in a layer near $\bar{x} = \bar{s}$. Then $\partial^2\bar{c}/\partial\bar{x}^2$ increases substantially so that it is no longer a small term compared to $(Pe/\bar{s})(\partial\bar{c}/\partial\bar{x})$.

To reveal the singular behavior of the true solution within the boundary layer, an "inner," or boundary variable y is introduced as follows (from here on all bar signs will be dropped from the dimensionless variables for simplicity unless otherwise stated):

$$y = Pe^{1/2}(s - x). \tag{29}$$

y is of the order of unity within the boundary layer. In the outer region, however, y is of the order of $Pe^{1/2}$. It is a common practice in boundary layer analysis to assume $y \to \infty$ in the outer region because $Pe \gg 1$ and the error introduced by such an approximation is of higher orders. The definition of the boundary variable (Eq. 29) can also be interpreted as a coordinate transformation from the fixed coordinates at the base to the moving coordinates at the tip of the pseudopod plus a stretch (by a factor of $Pe^{1/2}$). Substitution of Eq. 29 into Eqs. 28 leaves us with

$$\begin{cases} \dfrac{1}{Pe}\dfrac{\partial c}{\partial t} + \left[\dfrac{d}{dt}\left(\dfrac{s}{Pe^{1/2}}\right) - \left(\dfrac{Pe^{1/2}}{s}\right)\right]\dfrac{\partial c}{\partial y} = \dfrac{\partial^2 c}{\partial y^2} & \text{in} \quad 0 < y < \infty, t > 0, \\ \dfrac{\partial c}{\partial y} + \left(\dfrac{Pe^{1/2}}{s}\right)(c + C_1) = (c + C_2)\dfrac{d}{dt}\left(\dfrac{s}{Pe^{1/2}}\right) & \text{at} \quad y = 0, t > 0, \\ \dfrac{\partial c}{\partial t} - H\dfrac{\partial c}{\partial y} + c = 0 & \text{at} \quad y = 0, t > 0, \\ c = 1 & \text{as} \quad y \to \infty, t \geq 0, \\ c = 1 & \text{at} \quad t = 0, \\ s = 0 & \text{at} \quad t = 0, \end{cases} \tag{30}$$

in which

$$H = \frac{Pe^{1/2}}{Bi} = \left[\frac{K\phi(p_i - p_e + \eta\Delta\mu n/l)}{\mu C k_+ h^2}\right]^{1/2} \tag{31}$$

is the fractional depth of the reaction chamber which a convective G-actin penetrates in the time scale of actin polymerization.

Next the solution to Eqs. 30 is expanded into the following singular perturbation series:

$$\frac{s(t)}{Pe^{1/2}} \sim s_0(t) + \frac{1}{Pe}s_1(t) + \frac{1}{Pe^2}s_2(t) + \cdots, \cdots$$

$$c(x,t) \sim c_0(y,t) + \frac{1}{Pe}c_1(y,t) + \frac{1}{Pe^2}C_2(y,t) + \cdots, \cdots$$

$$\text{as } Pe \to \infty, \tag{32}$$

in which $(1/Pe)$ is taken as the small perturbation parameter. Substituting the series expansions 32 into Eqs. 30 and then equating the coefficients of like-powers of Pe to zero, yields the following sequence of equations:

Zeroth-order problem:

$$\begin{cases} \dfrac{\partial^2 c_0}{\partial y^2} + \left(\dfrac{1}{s_0} - \dfrac{ds_0}{dt}\right)\dfrac{\partial c_0}{\partial y} = 0 \quad \text{in} \quad y > 0, \\ c_0 = 1 \quad \text{as} \quad y \to \infty, \\ (c_0 + C_2)\dfrac{ds_0}{dt} - (c_0 + C_1)\dfrac{1}{s_0}\Big]_{y=0} = \dfrac{\partial c_0}{\partial y}\Big]_{y=0} \quad \text{in} \quad t > 0, \\ s_0 = 0 \quad \text{at} \quad t = 0, \\ \dfrac{\partial c_0}{\partial t} - H\dfrac{\partial c_0}{\partial y} + c_0\Big]_{y=0} = 0 \quad \text{in} \quad t > 0, \\ c_0 = 1 \quad \text{at} \quad t = 0; \end{cases} \tag{33}$$

First-order problem:

$$\begin{cases} \dfrac{\partial^2 c_1}{\partial y^2} + \left(\dfrac{1}{s_0} - \dfrac{ds_0}{dt}\right)\dfrac{\partial c_1}{\partial y} = \dfrac{\partial c_0}{\partial t} + \left(\dfrac{s_1}{s_0^2} + \dfrac{ds_1}{dt}\right)\dfrac{\partial c_0}{\partial y} \quad \text{in} \quad y > 0, \\ c_1 = 0 \quad \text{as} \quad y \to \infty, \\ (c_0 + C_2)\dfrac{ds_1}{dt} + \dfrac{c_0 + C_1}{s_0^2}s_1\Big]_{y=0} \\ \qquad = -\dfrac{\partial c_1}{\partial y} + \left(\dfrac{1}{s_0} - \dfrac{ds_0}{dt}\right)c_1\Big]_{y=0} \quad \text{in} \quad t > 0, \\ s_1 = 0 \quad \text{at} \quad t = 0, \\ \dfrac{\partial c_1}{\partial t} - H\dfrac{\partial c_1}{\partial y} + c_1\Big]_{y=0} = 0 \quad \text{in} \quad t > 0, \\ c_1 = 0 \quad \text{at} \quad t = 0; \end{cases} \tag{34}$$

It is worth noting that the time derivative of c_i drops out from the ith-order perturbation problem. Within the boundary layer the dominant balance is between convection and diffusion terms and the local change of concentration is one order of magnitude smaller (cf. the first equation of Eqs. 30). Thus t becomes a parameter rather than an independent variable in equations on c_i. One can therefore first solve the spatial dependence of c_i from the first two equations (of Eqs. 33 or 34), leaving s_i as an undetermined function of time and one arbitrary function of time of integration ($A(t)$ or $B(t)$ in Eqs. 35 or 36 below). Then s_i can be found from the next two equations (of Eqs. 33 or 34). The last two equations (of Eqs. 33 or 34) are used to determine the arbitrary function of time of integration.

The zeroth-order solution is

$$s_0(t) = \left(2\frac{1 + C_1}{1 + C_2}t\right)^{1/2}$$

$$c_0(y,t) = 1 + A(t)\exp\left(-\frac{\zeta y}{Ht^{1/2}}\right), \tag{35a}$$

where

$$A(t) = -1 + 2\zeta F(t^{1/2} + \zeta) + [1 - 2\zeta F(\zeta)]\exp(-t - 2\zeta t^{1/2})$$

$$\zeta = H(C_2 - C_1)[2(1 + C_1)(1 + C_2)]^{-1/2}, \tag{35b}$$

in which $F(z) = e^{-z^2}\int_0^z e^{u^2}\,du$ is the Dawson's integral (Abramowitz and Stegun, 1964).

The solution to the first-order problem is

$$s_1(t) = \frac{s_0(t)}{2(C_2 - C_1)}\frac{1}{t}\int_0^t [(2\tau + 2\zeta\tau^{1/2} - 1)A(\tau) + 2\tau]\,d\tau,$$

$$c_1(y,t) = \left[He^{-t-2\zeta t^{1/2}}\int_0^t B(\tau)e^{\tau + 2\zeta\tau^{1/2}}\,d\tau + B(t)y - \frac{A(t)}{4t}y^2\right]\exp\left(-\frac{\zeta y}{Ht^{1/2}}\right), \tag{36a}$$

where

$$B(t) = \frac{H}{\zeta}t^{1/2} + \frac{H}{\zeta}\cdot\left(\frac{2 + C_2}{1 + C_2}t^{1/2} + \zeta - \frac{1}{2}t^{-1/2}\right)A(t) + \frac{C_2 - C_1}{1 + C_1}\frac{s_1(t)}{2t}A(t) + \frac{H}{\zeta(1 + C_2)}\left(t^{1/2} + \zeta - \frac{1}{2}t^{-1/2}\right)A^2(t). \tag{36b}$$

Thus, to the first-order asymptotic approximation,

$$s(t) \approx Pe^{1/2}s_0(t) + Pe^{-1/2}s_1(t),$$

$$c(x,t) \approx c_0\{Pe^{1/2}[s(t) - x], t\} + \frac{1}{Pe}c_1\{Pe^{1/2}[s(t) - x], t\}.$$

$$\text{as } Pe \gg 1 \tag{37}$$

Note that the above "inner solution" matches the outer solution in the "outer limit," i.e., $c \sim 1$ as $y \to \infty$. It is

therefore also a uniform asymptotic solution to the true solution in the entire domain $0 \le x \le s$.

Higher-order terms in the asymptotic series are in principle obtainable by carrying out the perturbation procedure, but the complexity of calculations will increase rapidly with the increasing order. Higher order analysis will not be pursued here because Eqs. 35 and 36 are sufficient for the purpose of illustrating the behavior of the solution. Also, the first-order asymptotic approximate solution is accurate enough for *Pe* larger than one (cf. Section IV).

Similarity Solution for Long-Term Behavior

The time history of G-actin concentration at the tip of the pseudopod can be examined using just the zeroth-order approximate solution (Eqs. 35). Expanding the Dawson's integral into large t asymptotic series, the second equation of 35a yields

$$c(s,t) \approx c_0(0,t) = 2\zeta F(t^{1/2}+\zeta) + [1 - 2\zeta F(\zeta)]e^{-t-2\zeta t^{1/2}} \sim \frac{\zeta}{t^{1/2}+\zeta}\left[1 + \sum_{n=1}^{\infty} \frac{(2n-1)!!}{2^n}(t^{1/2}+\zeta)^{-2n}\right] \quad \text{as} \quad t \to \infty. \tag{38}$$

When $t \gg 1$, $c(s,t) \approx 0$. This suggests that the long-term behavior of the solution to Eqs. 28 can be approximated by the solution to a system defined by 28 except the third equation, which is replaced by $c(s,t) = 0$. Also, the fifth equation of 28 is no longer needed in the new system. However small this change is, the new system is now solvable in closed form. This is because the reference time scale, $(Ck_+)^{-1}$, of the original problem now drops out from the new problem and no dimensionless time or length variable can be constructed based on the (dimensional) parameters of the new problem. Hence t, x, and s must appear in dimensionless combinations of $(xt^{-1/2})$ and $(st^{-1/2})$ which are similarity variables. Defining new variables by

$$u = xt^{-1/2}/2, \quad c(x,t) = f(u), \quad s(t)t^{-1/2}/2 = \lambda, \tag{39}$$

Eqs. 28 with the third equation replaced by $c(s,t) = 0$ and the fifth equation deleted then reduce to the following system of ordinary equations:

$$\begin{cases} f'' + \left(2u - \dfrac{Pe}{\lambda}\right)f' = 0 \quad \text{in} \quad 0 < u < \lambda, \\ f = 1 \quad \text{at} \quad u = 0, \\ f = 0 \quad \text{at} \quad u = \lambda, \\ f' = \dfrac{PeC_1}{\lambda} - 2\lambda C_2 \quad \text{at} \quad u = \lambda, \end{cases} \tag{40}$$

the solution of which is

$$s(t) = 2\lambda t^{1/2},$$

$$c(x,t) = f(xt^{-1/2}/2) = 1 - \frac{\operatorname{erf}\left(xt^{-1/2}/2 - \dfrac{Pe}{2\lambda}\right) + \operatorname{erf}\left(\dfrac{Pe}{2\lambda}\right)}{\operatorname{erf}\left(\lambda - \dfrac{Pe}{2\lambda}\right) + \operatorname{erf}\left(\dfrac{Pe}{2\lambda}\right)},$$

$$\left(\lambda C_2 - \frac{Pe}{2\lambda}C_1\right)e^{(\lambda - Pe/2\lambda)^2} \cdot \left[\operatorname{erf}\left(\lambda - \frac{Pe}{2\lambda}\right) + \operatorname{erf}\left(\frac{Pe}{2\lambda}\right)\right] = \pi^{-1/2}, \quad \text{as } t \gg 1 \tag{41}$$

where $\operatorname{erf}(z) = 2\pi^{-1/2}\int_0^z e^{-u^2}\,du$ is the error function (Abramowitz and Stegun, 1964). Solution 41 gives an approximation to the solution of Eqs. 28 when the time is much greater than the relaxation time scale of actin polymerization.

It is worth noting that Eqs. 41 satisfy all but the fifth equation of 28. The long-term approximate solution differs from the exact solution in that c in Eqs. 41 is discontinuous at (0, 0). According to Eqs. 41, once the pseudopod growth begins the concentration of G-actin at the tip of the psuedopod drops immediately from the initial value of reservoir concentration to the critical concentration of polymerization. In contrast the tip concentration of the true solution decays algebraically with time ($\sim t^{-1/2}$) to the critical concentration, as demonstrated by the perturbation solution (Eq. 38) (cf. Fig. 5).

Solution 41 is valid for all values of *Pe*, large or small. When *Pe* is large, the long-term solution can be compared with the perturbation solution 35–37 by expanding 41 into asymptotic series of powers $(1/Pe)$ siimlar to 32. Neglecting terms of higher order than $(1/Pe)$ and converting the variable into y by using Eq. 29, Eqs. 41 yield

$$s \sim \left(2\frac{1+C_1}{1+C_2}Pet\right)^{1/2}\left[1 + \frac{1}{2Pe(C_2 - C_1)}\right],$$

$$c \sim 1 - \left\{1 - \frac{1}{Pe}\left[\frac{\zeta(C_1 + C_2 + 2C_1C_2)}{H(C_2 - C_1)^2}\frac{y}{2t^{1/2}} + \frac{y^2}{4t}\right]\right\} \cdot \exp\left(-\frac{\zeta y}{Ht^{1/2}}\right), \quad \text{as} \quad Pe \to \infty, \quad t \gg 1, \tag{42}$$

in which H and ζ are defined by Eq. 31 and the second equation of 35b, respectively, and ζ/H depends on C_1 and C_2 only. It can be shown that as $t \to \infty$, Eqs. 35–37 approach 42 the corresponding like-powers of *Pe* term by term, as expected.

When *Pe* is much smaller than unity, diffusion overwhelms convection in G-actin transport. In this case, a regular perturbation analysis using *Pe* as a small parameter in Eqs. 28 has not been as successful. Even the zeroth-order problem is not solvable in closed form. However, the behavior of the solution of Eqs. 28 when $Pe \ll 1$ can be examined by using the long-term approximation of

Eqs. 41. Taking the limit $Pe \to 0$ results in

$$s(t) = 2\lambda_0 t^{1/2},$$

$$c(x, t) = 1 - \frac{\text{erf}\,(xt^{-1/2}/2)}{\text{erf}\,(\lambda_0)},$$

$$\lambda_0 e^{\lambda_0^2}\,\text{erf}\,(\lambda_0) = \pi^{-1/2} St, \tag{43}$$

in which $St = 1/C_2$ is the mass transfer Stefan number. This is the well known solution to the Stefan problem (e.g., Crank, 1984). It is a fundamental property of the Stefan problem that the growth s is proportional to $t^{1/2}$. For the present moving boundary problem, this is to be expected in diffusion-dominated cases because then the present moving boundary model resembles that of Stefan's. Of interest is that in convection-dominated cases the long-term behavior also has such a property, as can be seen from Eqs. 41. This results from the increasing resistance to the flow through the solid network as the pseudopod grows.

IV. COMPARISON OF THE THEORY WITH EXPERIMENTS

In this section the relevance of the solutions of the moving boundary model obtained in Section III to biological problems is evaluated by calculating sample cases with realistic biological parameters and comparing the computed results with experimental data. The solutions are applied to two different systems. One is pseudopod protrusion in leukocytes and the other is elongation of acrosomal process in *Thyone* sperms.

Estimation of Physical Parameters

The measured diameter, d, of actin microfilaments is about 6–8 nm (Pryzwansky et al., 1983). The measured spacing between filaments, h, ranges from 20 nm (Luby-Phelps et al., 1986) to 100 nm (Hartwig and Shevlin, 1986). The typical values of $d = 7$ nm and $h = 50$ nm are chosen here. The latter is also chosen as the thickness of the reaction chamber at the tip of the pseudopod. The porosity of the F-actin network and the surface number density of actin filament ends at the growing tip of a pseudopod estimated from these geometrical data are, respectively, $\phi = 0.954$ and $n = 4 \times 10^{10}/\text{cm}^2$. Each filament is composed of 370 protomers per micron (Glenney et al., 1981; Aebi et al., 1981). Hence the length that a filament extends when a monomer adds to it is $l = 2.7 \times 10^{-7}$ cm. The total actin concentration in cortical cytoplasm has been estimated to range from 10 to 20 mg/ml (Stossel, 1988), of which as much as 50–70% is unpolymerized in unstimulated leukocytes (Carson et al., 1986). A typical value of the G-actin concentration at the base of the pseudopod is chosen to be $c_1 = 7$ mg/ml $= 167\ \mu\text{M} = 10^{17}/\text{cm}^3$. (G-actin has a molecular weight of ~42,000 [Stossel et al., 1981].) The polymerization reaction rate constants of ATP–actin at barbed ends have been measured to be $k_+ = 11.6\ \mu\text{M}^{-1}\ \text{s}^{-1} = 1.93 \times 10^{-14}\ \text{cm}^3\ \text{s}^{-1}$ and $k_- = 1.40\ \text{s}^{-1}$ (Pollard, 1986). Using the above values, the two dimensionless concentration parameters defined in Eqs. 27 are computed to be

$$C_1 = 7.27 \times 10^{-4}, \quad C_2 = 1.56. \tag{44}$$

The cellular molar ratio of capping protein to actin in *Acanthamoeba* has been estimated to be ~1:150. Approximately one-third of the capping proteins have been found to localize within cell cortex and to band with the plasma membrane (Cooper et al., 1984). Hence the total concentration of capping protein in the cell periphery is of the order of 1 μM. Gelsolin has also been found to reside in the cortical cytoplasm and to be concentrated in pseudopod of leukocytes during phagocytosis (Yin et al., 1981). If one assumes that the gelsolin concentration at the tip of a pseudopod in leukocytes is of the same order of magnitude as capping protein in the periphery of *Acanthamoeba*, i.e., $c_p = 1\ \mu\text{M} = 6.02 \times 10^{14}/\text{cm}^3$, then using the measured equilibrium constant $K_d = 10^7$–$10^9\ \text{M}^{-1}$, for binding of gelsolin to actin filament barbed ends (Janmey et al., 1985), the number density of free barbed ends of actin filaments can be computed from Eq. 14. This gives a value of $C = 7.40 \times 10^{15}/\text{cm}^3$, indicating that only a very small fraction (7.5%) of the total ends are capped. However, it is possible that when the process of pseudopod protrusion is initiated, gelsolin "flows" along the plasma membrane towards the tip of the growing pseudopod. The c_p value may then increase substantially within the reaction zone at the tip of the pseudopod and as a result, a large number of filament ends may be capped.

The characteristic relaxation time scale of actin polymerization calculated using $C = 7.40 \times 10^{15}/\text{cm}^3$ is $(Ck_+)^{-1} = 7.02 \times 10^{-3}$ s. This result indicates that the assembly process is rapid and the control of the pseudopod growth lies elsewhere. The short relaxation time constant comes about because the concentration of the free filament barbed ends, C, at the polymerization pool is very high when the concentration of gelsolin at the tip of the pseudopod is only $c_p = 1\ \mu\text{M}$.

The diffusion coefficient of G-actin in aqueous solution has been found to be $\sim 7 \times 10^{-7}\ \text{cm}^2/\text{s}$. However, the measured D values in cytoplasm of living cells vary from 10^{-7} to $10^{-9}\ \text{cm}^2/\text{s}$ (see Section I). Inclusion of effects such as increase of the Stokes' radius of unpolymerized actin due to forming a complex with profilin (which reduces the diffusion coefficient ~10%) and the steric obstruction of the microtrabecular lattice in cytoplasm (which retards the motion of the particles further by ~20%) still cannot explain the discrepancies of the different values of D (e.g., see Jacobson and Wojcieszyn, 1984; Gershon et al., 1985). The value of $D = 10^{-8}\ \text{cm}^2/\text{s}$ measured by Felder (1984) is chosen here. The mass transfer Biot number computed from Eq. 26 using $D = 10^{-8}\ \text{cm}^2/\text{s}$ is

$$Bi = 0.626. \tag{45}$$

The viscosity of the fluid suspension, μ, is albeit a little larger than, but of the same order as, that of water, which is 10^{-2} dyn · s/cm^2. The permeability, K, of the F-actin network seems not to have been measured experimentally. This quantity is estimated here using the Kozeny-Carman theory (e.g., see Curry, 1986):

$$K = \frac{d^2\phi^3}{80(1-\phi)^2} = 2.49 \times 10^{-12}\ \text{cm}^2, \qquad (46)$$

where d and ϕ are, respectively, the diameter of actin filament and the porosity of the F-actin network. Values of K similar to those given by Eqs. 46 and 49 (see below) can also be obtained from structural models of the F-actin networks and the "drag theory" based on low Reynolds number hydrodynamics (Happel and Brenner, 1973, pp. 392–395).

The transcellular pressure difference, $p_e - p_i$, between the external medium and the main cell body is assumed to be zero for a leukocyte suspended freely in isotonic solution. Thermodynamics measurement of the free energy change of actin polymerization gives a value of $\sim\Delta\mu = 6$ kcal/mol $= 4.2 \times 10^{-13}$ dyn · cm (Hill, 1981; Gordon et al., 1976).

The only other datum needed for numerical computations but not available in the literature is the efficiency, η, of energy transduction from chemical potential to mechanical work. The value of η is needed for calculation of the mass transfer Peclet number, Pe, and the convective fractional depth, H. In the present estimate, the value of η is determined by comparing the theoretical solutions with experimentally observed time courses of pseudopod protrusion.

Comparison of Theoretical Curves with Experimental Data

Schmid-Schönbein et al. (1982) have observed and reported the time courses of pseudopod formation in leukocytes. Their experimental data are shown in Fig. 2. Also plotted in Fig. 2 is a theoretical curve of the present model. The theoretical curve is computed using (the dimensional form of) the first equation, $s(t) = 2\lambda(Dt)^{1/2}$, of solution 41 because the time scale of pseudopod protrusion (tens of seconds) is very large compared to the time scale of actin polymerization (milliseconds). It follows that the long-term approximation is usually valid.

Fitting the theoretical curve with the experimental data allows determination of a best fit value of λ (= 0.63). The mass transfer Peclet number is then determined from the third equation of 41, which defines implicitly Pe as a function of λ, C_1, and C_2 by a transcendental equation. Fig. 3 shows curves of Pe versus λ with the parameter values of C_1 and C_2 given by Eqs. 44 and 50 (see below) according to the third equation of 41. The best Pe corresponding to the best fit λ is $Pe = 0.984$. This Pe value indicates that according to the present model, convection is just as important as diffusion in supplying the G-actin for pseudopod growth at the tip.

The efficiency η can now be solved from Eq. 25 and then computed using the value $Pe = 0.984$ and values of other quantities estimated previously. The result is

$$\eta = \frac{l}{n\Delta\mu}\left[\frac{\phi\mu D}{K}Pe - (p_i - p_e)\right] = 6.1 \times 10^{-4}. \qquad (47)$$

The low efficiency implies that dissipation consumes most of the free energy liberation, which is consistent with the fact that actin polymerization is a strongly endothermic and entropy driven process (Gordon et al., 1976). It leaves open the possibility that a slower protrusion at higher efficiency may allow the pseudopod to grow (push) against a considerable external pressure as in the case of a leukocyte-penetrating small blood vessel into interstitium. In such a case, the transcellular pressure difference, $(p_i - p_e)$, is negative and opposes the protrusion. More

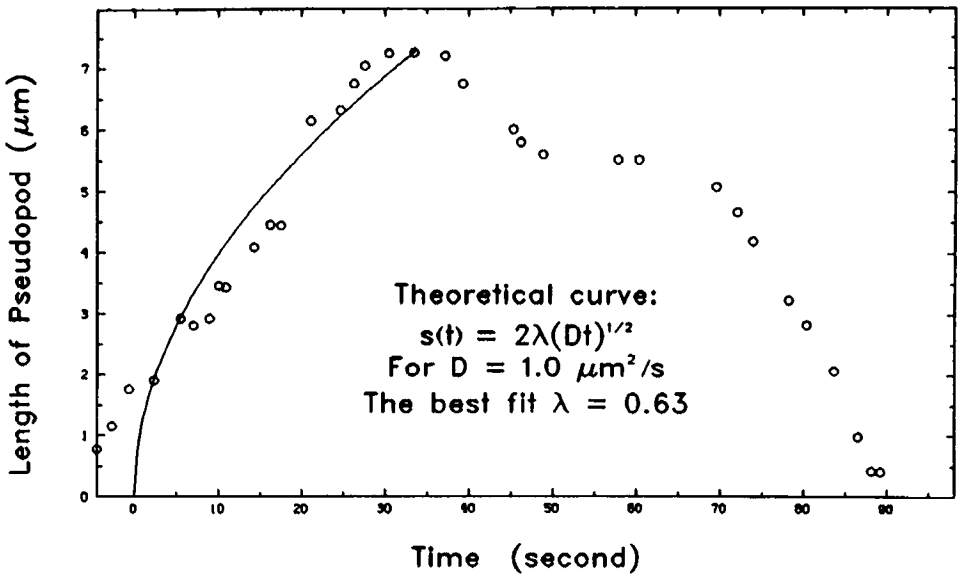

FIGURE 2 Time course of pseudopod protrusion in a human neutrophil. The experimental data are from Schmid-Schönbein et al. (1982). The theoretical curve is computed using the first equation of the long-term solution (Eqs. 41) with diffusion coefficient $D = 10^{-8}$ cm^2/s and $\lambda = 0.63$ which gives the best fit of the data.

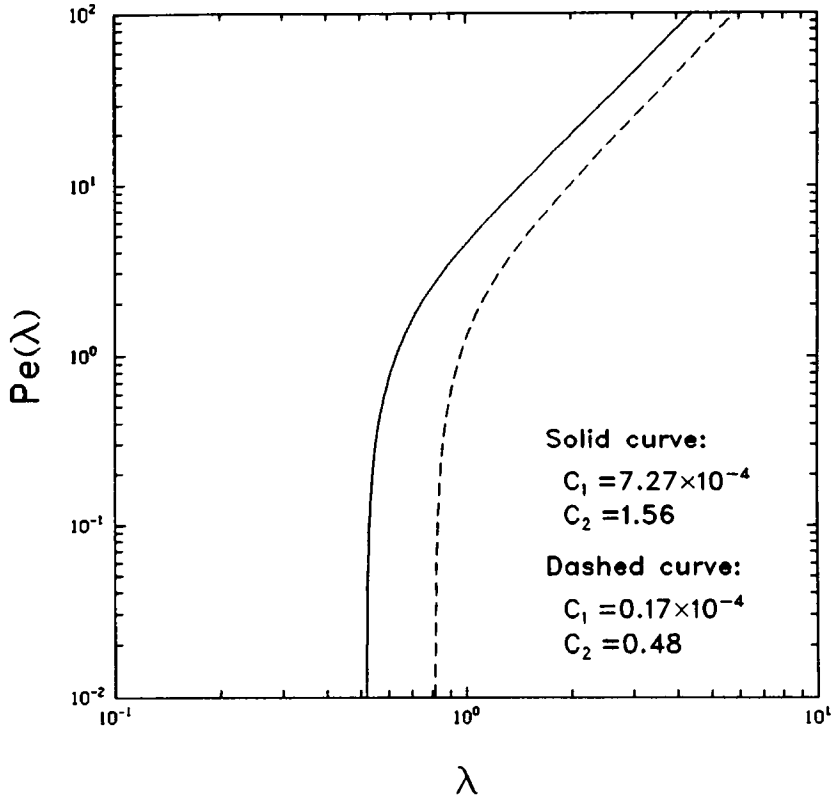

FIGURE 3 Curves of *Pe* versus λ as defined implicitly by a transcendental equation, the third equation of Eqs. 41, with parameters given respectively by Eqs. 44 and 50. *Solid curve*, $C_1 = 7.27 \times 10^{-4}$; $C_2 = 1.56$. *Dashed curve*, $C_1 = 1.65 \times 10^{-5}$; $C_2 = 0.479$.

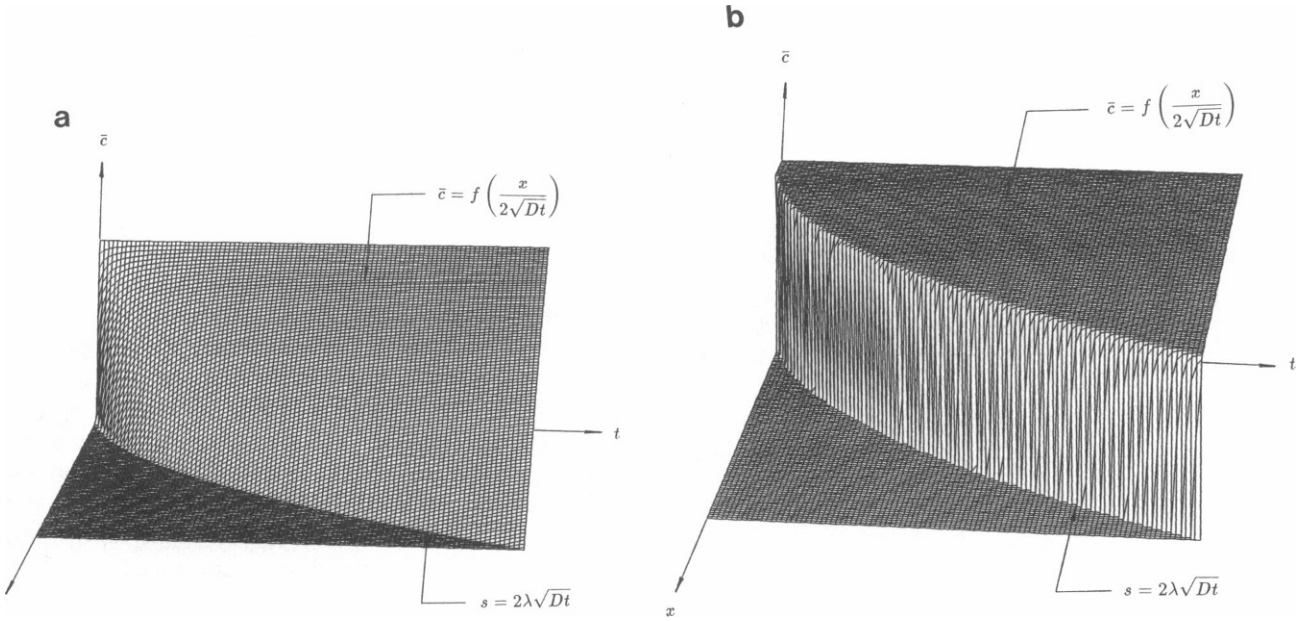

FIGURE 4 Spatial and temporal concentration distribution of G-actin in (*a*) a growing pseudopod of a leukocyte and (*b*) an elongating acrosomal process in a *Thyone* sperm as shown by 3-D surfaces in the $(x, t, \bar{c})$ space. The surfaces are computed using the second equation of the long-term solution (Eqs. 41) with the dimensionless concentration variable, $\bar{c}$ defined by Eq. 24, dimensional x and t, and the diffusion coefficient $D = 10^{-8}$ cm^2/s. Parameters are, respectively, (*a*) $\lambda = 0.64$, $Pe = 0.984$, and (*b*) $\lambda = 15.3$, $Pe = 694$. The time courses of tip location of the projections (pseudopod in *a* and acrosomal process in *b*) are shown by the curves $s = 2\lambda(Dt)^{1/2}$ on the x-t plane, which are the intersecting curves of the surfaces $\bar{c} = f[x(Dt)^{-1/2}/2]$ and the x-t plane. No boundary layer near the growing tip of pseudopod can be seen in *a* because the mass transport Peclet number is only $Pe = 0.984$. In contrast, a very thin boundary layer is developed near the growing tip of the acrosomal process in *b* because in the present case the mass transport Peclet number is $Pe = 694$, which indicates a convection-dominated G-actin transport.

work is done for the same rate of growth and as a result, higher efficiency is needed.

Fig. 4 *a* shows the spatial and temporal concentration distribution of G-actin as a 3-D surface in the (dimensional) (x, t, $\bar{c}$) space using the second equation of the long-term solution (Eqs. 41). The curve defined by the intersection of the surface $\bar{c} = f[x(Dt)^{-1/2}/2]$ and the x-t plane is the location of the growing tip, $s = \lambda(Dt)^{1/2}$. The boundary layer of the concentration profile does not develop because the mass transfer Peclet number is only 0.984.

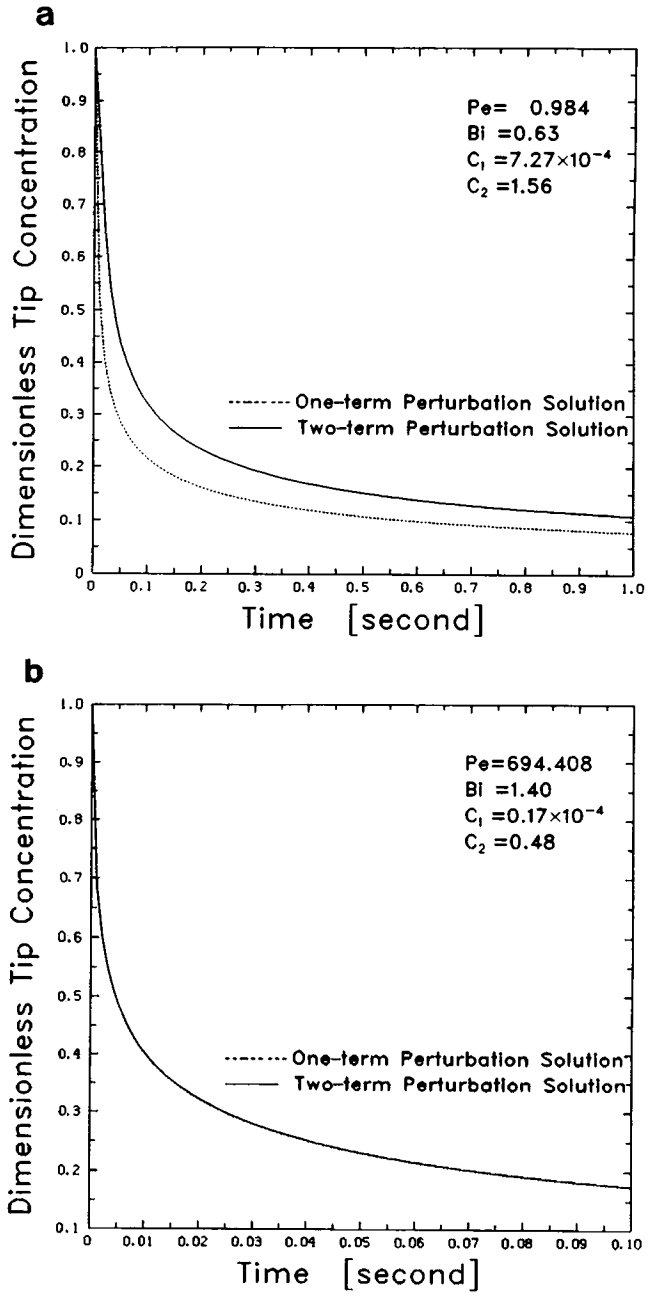

FIGURE 5 Time history of G-actin concentration at tip of (*a*) the pseudopod in leukocytes and (*b*) the acrosomal process in *Thyone* sperms. The curves are computed using the perturbation solutions (Eqs. 35–37). *Dashed curves*, zeroth-order (one-term) perturbation approximation. *Solid curves*, first-order (two-term) perturbation approximation. The reference time scales are, respectively, (*a*) $(Ck_+)^{-1} = 7.02 \times 10^{-3}$ s for pseudopod protrusion in leukocytes and (*b*) $(Ck_+)^{-1} = 1.6 \times 10^{-4}$ s for acrosomal elongation in *Thyone* sperms. Parameters are, respectively, (*a*) $Pe = 0.984$, $Bi = 0.626$, $C_1 = 7.27 \times 10^{-4}$, $C_2 = 1.56$; and (*b*) $Pe = 694$, $Bi = 1.40$, $C_1 = 1.65 \times 10^{-5}$, $C_2 = 0.479$. The two curves in *b* are so close as to become undistinguishable.

To verify that the long-term solution (Eqs. 41) is a valid approximation, the time history of G-actin concentration at the tip of the pseudopod is plotted on Fig. 5 *a* using the perturbation solutions (Eqs. 35–37), parameter values of C_1 and C_2 given by Eqs. 44, Bi by Eq. 45, the best fit value $Pe = 0.984$, and the reference time scale $(Ck_+)^{-1} = 7.02 \times 10^{-3}$s. It can be seen that within 1 s, the dimensionless tip concentration of actin monomers drops from 1 to ~0.1. That is, after 1 s, G-actin concentration in the reaction pool at the tip of the pseudopod drops from its initial value of the reservoir concentration to a value close to the critical concentration of actin polymerization (within 10%). Thus the long-term solution, according to which the tip concentration of G-actin jumps from 1 to 0 at $t = 0$, is approximate when t is greater than 1 s.

Fig. 6 *a* shows the relative errors of tip location between perturbation and long-term solutions, and long-term solution and its large Pe two-term asymptotic approximation. The solid curve and the dashed horizontal line are, respectively, $|(s_p - s_l)/s_p|$ versus t and $|(s_a - s_l)/s_a|$ versus t, where s_p, s_l, and s_a denote, respectively, the two-term perturbation solution given by the first equation of 37, the long-term solution given by the first equation of 41, and the two-term asymptotic approximation of the long-term solution given by the first equation of 42, all in dimensional forms. It is very interesting to observe that even though $Pe = 0.984$ is slightly smaller than unity, the relative error between the long-term solution and its two-term asymptotic approximation is only ~8% (*dashed horizontal line*). It demonstrates the power of perturbation methods. (The solution 42 can also be obtained by using the same perturbation procedure on Eqs. 40 as that used on Eqs. 30 to obtain solution 37.) It is a common experience in perturbation analysis that the accuracy of the approximate solutions sometimes goes beyond the assumed domain of the perturbation parameter. Also, the rapid drop of the relative error between the perturbation and long-term solutions (*solid curve*) to its asymptote (*dashed horizontal line*) confirms the validity of the long-term solution, since the relative error which arises from the long-term approximation is <0.6% a second after the pseudopod growth begins.

Application of the Model to Other Systems

Although the present work is primarily developed to model pseudopod protrusion in leukocytes, the model is applicable to growth of other cellular systems containing actin matrix as well, for instance, the extension of acrosomal process in sperm cells. Tilney and Inoué (1982) have collected most

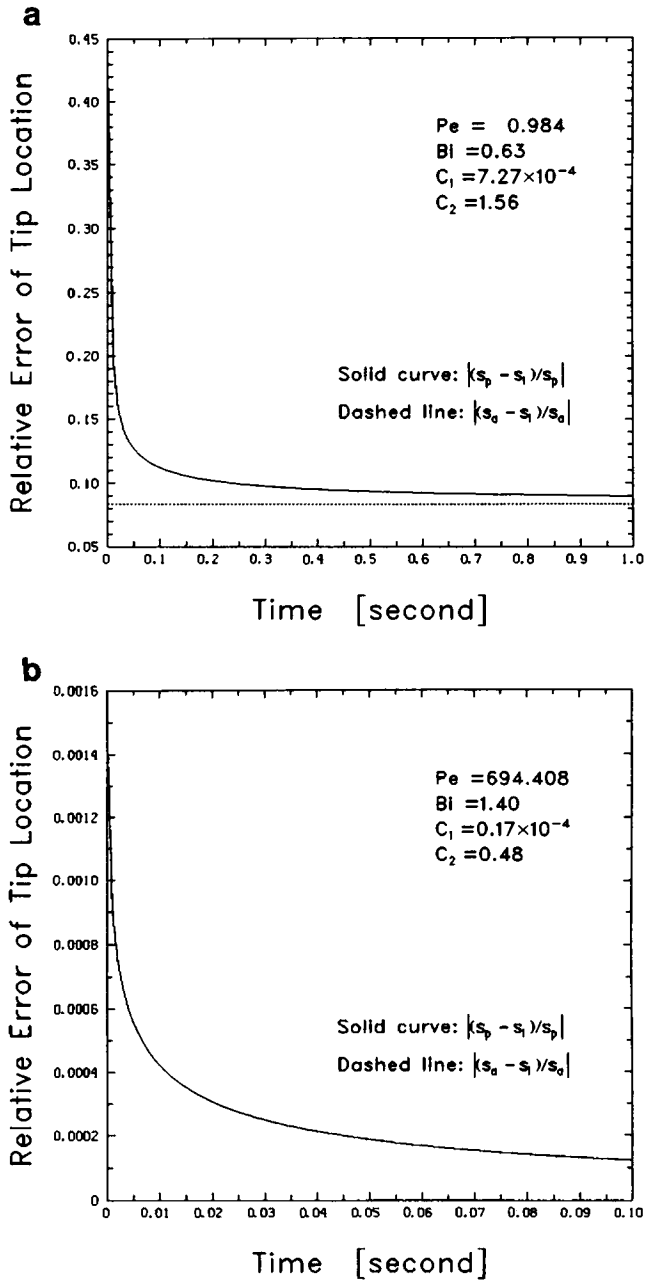

FIGURE 6 Comparison of perturbation with long-term solutions of the location of the growing tip of (*a*) pseudopod in leukocytes and (*b*) acrosomal process in *Thyone* sperms. *Solid curves*, relative error of tip location, $|(s_p - s_l)/s_p|$, between long-term solution, s_l, given by the first equation of 41 and the two-term perturbation solution, s_p, given by the first equation of 37. *Dashed lines*, relative error of tip location, $|(s_a - s_l/s_a|$, between long-term solution, s_l, and its two-term asymptotic approximation, s_a, given by the first equation of 42. The reference time scales and parameters are the same as those given in Fig. 5. The dashed horizontal line in *b* is superimposed onto the abscissa because the relative error is only in the order of 10^{-7}.

of the experimental data for acrosomal process in *Thyone* sperms needed for computation. Those which differ from their counterparts in leukocytes are quoted below (see also Perelson and Coutsais, 1986). The computations of h, n, and ϕ are based on the measurements that acrosomal processes have an average cross-sectional area of $\sim 1.3 \times 10^{-10}\text{cm}^2$, which contains on average 60 filaments.

$$c_i = 4.4 \times 10^{18}/\text{cm}^3, \quad h = 1.5 \times 10^{-6}\,\text{cm},$$
$$n = 4.7 \times 10^{11}/\text{cm}^2, \quad \phi = 0.82,$$
$$C = 3.2 \times 10^{17}/\text{cm}^3, \quad (Ck_+)^{-1} = 1.6 \times 10^{-4}\,\text{s}, \tag{48}$$

and

$$K = \frac{d^2\phi^3}{80(1-\phi)^2} = 1.04 \times 10^{-13}\text{cm}^2. \tag{49}$$

The corresponding dimensionless parameters are

$$C_1 = 1.7 \times 10^{-5}, \qquad C_2 = 0.48, \tag{50}$$

$$Bi = 1.4. \tag{51}$$

Since the value of relaxation time constant of actin polymerization, $(Ck_+)^{-1}$, is very small, the long-term solution is used to fit the experimental data. In Fig. 7 *a* the square of the length of the acrosomal process, $s^2(t)$, is plotted against time t according to (dimensional form of) the first equation of the solution 41, along with the experimental data measured by Tilney and Inoué (1982). For $D = 10^{-8}$ cm^2/s, the best fit value is $\lambda = 15.3$. The corresponding mass transfer Peclet number, obtained from the dashed curve in Fig. 3 which defines $Pe = Pe(\lambda)$ by the third equation of 41 with parameters C_1 and C_2 given by 50, is $Pe = 694$. The efficiency computed using Eq. 47 and the appropriate values of the quantities involved is $\eta = 0.75$. The high efficiency obtained in this case indicates that most of the chemical free energy liberated from actin polymerization is needed to draw sufficient G-actin supplies to the tip to catch the rapid growth of acrosomal process. The resulting relatively high efficiency, $\eta = 0.75$, is possibly due to the great regularity of actin filaments arranged within the acrosomal process.

Fig. 4 *b* is a counterpart of Fig. 4 *a* in the acrosomal process. The boundary layer of the G-actin concentration profile is a very thin layer in this case because $Pe = 694$ which indicates a convection dominated G-actin transport. It can be seen that the $\bar{c}$ surface is flat ($\bar{c} \approx 1$) within the region bounded by the intersecting curve $s = 2\lambda(Dt)^{1/2}$ and the t axis until it comes very close to the curve $x = s(t)$ where the $\bar{c}$ surface drops down nearly vertically to zero.

The large Pe value and narrow boundary layer suggest that the perturbation solution can be used for growth of acrosomal process. Both (dimensional forms of) the long-term and perturbation solutions, and the experimental data of Tilney and Inoué (1982) are plotted in Fig. 7 *b*. The perturbation solutions are computed according to Eqs. 35–37, using parameter values of C_1 and C_2 given by 50, Bi by 51, the best fit value $Pe = 694$, and the reference time scale $(Ck_+)^{-1} = 1.6 \times 10^{-4}$ s. Even though the Pe value is fitted using the long-term solution instead of the perturbation solution themselves, the three solutions, namely, one-

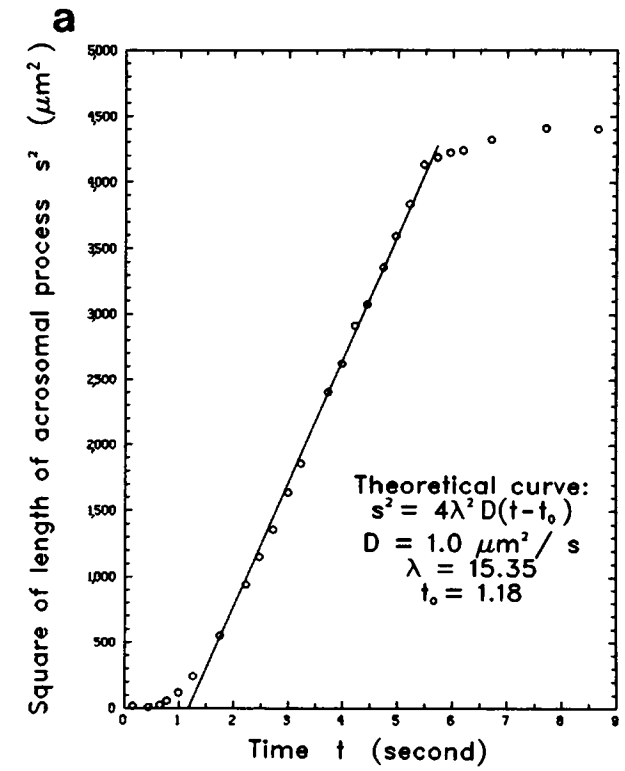

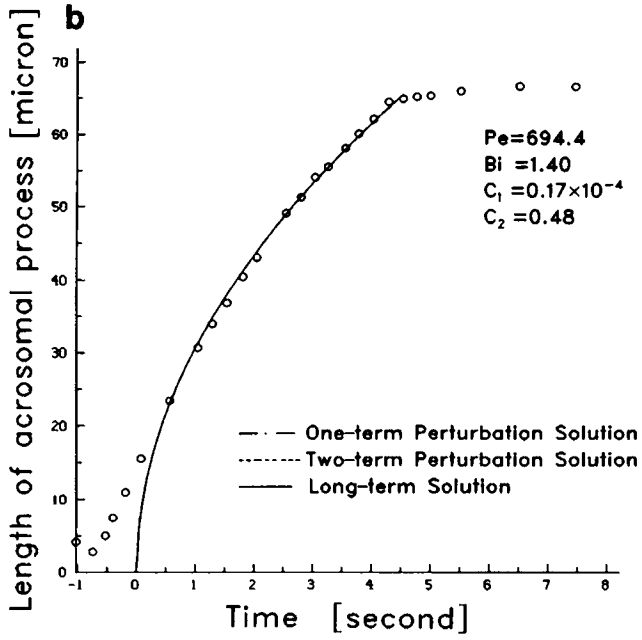

FIGURE 7 Time course of growth of acrosomal process in *Thyone* sperms. The experimental data were measured by Tilney and Inoué (1982). (*a*) Plot of the square of the length of acrosomal process against time. The theoretical line is computed using the long-term solution (Eqs. 41) with diffusion coefficient $D = 10^{-8}$ cm²/s and $\lambda = 15.3$ which gives the best fit to the data. (*b*) Plot of s versus t. The theoretical curves are computed using the perturbation solutions (Eqs. 35–37), with reference time scale $(Ck_+)^{-1} = 1.6 \times 10^{-4}$ s and parameters $Pe = 694$, $Bi = 1.40$, $C_1 = 1.65 \times 10^{-5}$, and $C_2 = 0.479$, and the long-term solution (Eqs. 41) with $\lambda = 15.3$. All three solutions, namely, long-term approximation, one- and two-term perturbation approximations, are superimposed onto a single curve, because the magnitude of the errors among them are less than the thickness of the curve.

term perturbation solution, two-term perturbation solution, and long-term solution, all fall into a single curve. The differences among the three solutions are within the width of the curve.

The time history of tip concentration of G-actin computed from (the dimensional forms of) the perturbation solutions 35–37 is plotted in Fig. 5 *b*. The tip concentration shows a rapid drop once the acrosomal process starts to elongate. Fig. 5 *b* differs from Fig. 5 *a* in that the two curves of one- and two-term perturbation solutions are almost undistinguishable. This is because in this large *Pe* (=694) case, just the zeroth-order perturbation solution is accurate enough and the first-order correction is very small. This feature is also demonstrated in Fig. 6 *b* in which $|(s_p - s_1)/s_p|$ and $|s_a - s_1)/s_a|$ are plotted against t. The relative error between the two-term perturbation and the long-term solutions of the tip location (*solid curve*) is orders of magnitude smaller in Fig. 6 *b* than that in Fig. 6 *a*. The relative error of tip location between the long-term solution and its two-term asymptotic approximation is of the order of 10^{-7}. The dashed horizontal line cannot be seen in the figure because it coincides with the abscissa. The good agreement among various solutions and between the theory and experiment suggest that the model is valid.

V. DISCUSSION AND CONCLUSION

A number of simplifying assumptions have been made during the development of the model. Some of them are straightforward, for example, the incompressibility assumption for fluid flow, assumption of negligible membrane tension, etc. Others, however, are non-trivial and therefore demand further exploration. In this section the model will be generalized to a 3-D formulation and the assumptions will be re-examined.

Generalization to Three-dimensional Formulation

Fig. 8 shows the 3-D domain under consideration in which the pseudopod consists of an interior, Ω, a base surface, $\partial\Omega_b$, a tip surface, $\partial\Omega_t$, and a sidewall surface $\partial\Omega_w$. The generalizations of Eqs. 1, 2, and 4 are straightforward. They are,

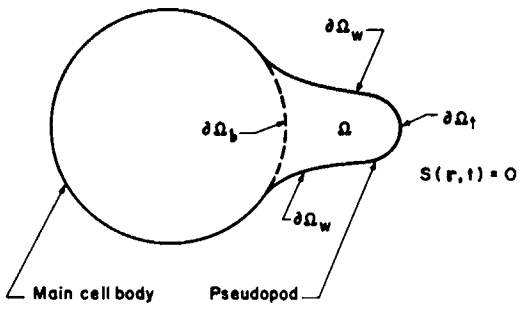

FIGURE 8 Schematic illustration of the domain and boundaries of a three-dimensional pseudopod in an active leukocyte.

respectively,

$$\nabla \cdot \mathbf{v} = 0 \quad \text{in} \quad \mathbf{r} \in \Omega, \tag{52}$$

$$\frac{\partial c}{\partial t} + \mathbf{v} \cdot \nabla c = D\nabla^2 c \quad \text{in} \quad \mathbf{r} \in \Omega, \tag{53}$$

$$\mathbf{v} = -\frac{K}{\phi\mu}\nabla p \quad \text{in} \quad \mathbf{r} \in \Omega, \tag{54}$$

where ∇ denotes the gradient operator. The generalizations of Eqs. 3 and 11 are more subtle. Let the shape of the tip surface, $\partial\Omega_t$, at any time instant be denoted by $S(\mathbf{r}, t) = 0$ such that its unit outward normal is $(\nabla S/|\nabla S|)$. The velocity of the growing front is

$$\mathbf{v}_0 = -\frac{\partial S}{\partial t}\frac{\nabla S}{(\nabla S)^2} \quad \text{on} \quad S = 0. \tag{55}$$

The 3-D counterparts of Eqs. 3 and 11 are, respectively,

$$\phi'(D\nabla c - \mathbf{v}c) \cdot \nabla S = \left(\frac{n}{l} + \phi c\right)\frac{\partial S}{\partial t} \quad \text{on} \quad S = 0, \tag{56}$$

$$\frac{\partial c}{\partial t} + \left(\frac{D/h}{|\nabla S|} - \frac{\partial S/\partial t}{(\nabla S)^2}\right)\nabla S \cdot \nabla c = -C(k_+ c - k_-) \quad \text{on} \quad S = 0, \tag{57}$$

in which C is given by Eq. 14.

Eqs. 7 and 16–18 still hold in 3-D cases, and are restated here:

$$p = p_e - \eta\nabla\mu\frac{n}{l} \quad \text{on} \quad S = 0, \tag{58}$$

$$p = p_i \quad \text{on} \quad \mathbf{r} \in \partial\Omega_b, \tag{59}$$

$$c = c_i \quad \text{on} \quad \mathbf{r} \in \partial\Omega_b, \tag{60}$$

and

$$c = c_i \quad \text{at} \quad t = 0. \tag{61}$$

The initial condition (19) is replaced by

$$S(\mathbf{r}, t) = S_0(\mathbf{r}) \quad \text{at} \quad t = 0, \tag{62}$$

where $S_0(\mathbf{r}) = 0$ is the initial shape of the tip surface of the pseudopod. The boundary conditions on the sidewall of the pseudopod $\partial\Omega_w$ are that the wall is impermeable to both the fluid suspension and the solute.

$$v_\nu = -\frac{K}{\phi\mu}\frac{\partial p}{\partial \nu} = 0 \quad \text{on} \quad \mathbf{r} \in \partial\Omega_w, \tag{63}$$

and

$$\frac{\partial c}{\partial \nu} = 0 \quad \text{on} \quad \mathbf{r} \in \partial\Omega_w, \tag{64}$$

in which v_ν is the normal component of fluid velocity and $\partial/\partial\nu$ denotes a normal derivative on the sidewall surface.

Examination of Simplifying Assumptions

Eq. 1 and its 3-D counterpart Eq. 52 imply that the fluid volume fraction or porosity of the actin network, ϕ, is a constant. The value of ϕ depends on time and position if there is conversion of material between fluid and solid phases throughout the volume, or if the actin microfilament network is subject to collapse or inflation due to deformation. That actin polymerization occurs only at the tip of the pseudopod by adding monomers to the preexisting filament barbed ends, without any spontaneous nucleation or fragmentation and reannealing of F-actin network inside the shaft of the pseudopod, has been strongly suggested by many experimental observations. The pseudopod protrusion is therefore said to be a surface growth rather than a volumetric growth. Thus asuming ϕ to be constant implies that the actin network merely provides a rigid porous scaffolding through which the fluid filters. Inclusion of deformation of the solid phase, which would be perhaps more realistic, is not very difficult in principle (for example, see Lanir, 1987*a*,*b*). However, it seems simpler to avoid the formidable mathematical complexity raised in biphasic formulation unless otherwise important physics would be missing, which does not seem likely in this case.

The treating of the complex cytoplasmic fluid phase as a solution of single solute also needs justification. The homogeneous solvent assumption is based on the fact that relaxation time scales of equilibrium for various components in the solvent are much smaller than the time scale of the motion under consideration. Therefore, all species in the solvent share common thermodynamical and mechanical features on the time scale of pseudopod formation. As far as the solute is concerned, G-actin is only one of the many proteins involved in the polymerization reaction. Other regulatory proteins such as profilin and actin-binding protein also come into play. However, no attempt to distinguish among these proteins is made at the present stage of modeling. Rather, the whole entity is represented by a single composite surrogate of which unpolymerized actin is the principal solute.

The term "unpolymerized actin" used here stands for both G-actin and profilin–actin complex. The actin monomer binding reaction

$$\text{G-actin} + \text{Profilin} \rightleftharpoons \text{Profilactin} \tag{65}$$

can be described in its equilibrium state by the following equation (e.g., Tobacman and Korn, 1982; Pollard and Cooper, 1984; Lal and Korn, 1985):

$$\frac{[\text{G-actin}][\text{Profilin}]}{[\text{Profilactin}]} = K_D. \tag{66}$$

As discussed in the Introduction, in the main cell body and in the shaft of the pseudopod most of unpolymerized actin is profilactin which prevents actin monomers from spontaneously polymerizing in undesired sites with high concen-

tration. At the tip of the pseudopod, on the other hand, the turnover of phosphoinositols that follows the binding of ligands to cell surface receptors releases actin monomers bound to profilin (Lassing and Lindberg, 1985). This process is modeled here by assuming all unpolymerized actin within the pseudopod is profilactin, whereas at the growing tip it is G-actin. It is a simplification such that the spatial distribution of the equilibrium constant for binding profilin to G-actin is idealized to be zero all the way along the shaft of the pseudopod and to be infinity at the tip of the pseudopod. That is,

$$K_D(x) = hP\delta(x - s), \tag{67}$$

where h is the thickness of the reaction chamber at the growing tip and $\delta(\cdot)$ is Dirac delta. P stands for the concentration of total profilin. P is approximately equal to the concentration of free profilin because the free profilin concentration is much higher than the concentration of bound profilin (Pollard and Cooper, 1984). Eq. 67 allows the use of the same notation c for concentrations of both profilactin and G-actin. Because along the shaft, [G-actin] = 0 and [Profilactin] = c, while at the tip, [Profilactin] = 0 and from Eqs. 66 and 67,

$$[\text{G-actin}] = \frac{1}{h}\int_{s-h}^{s} \frac{[\text{Profilactin}]}{[\text{Profilin}]} K_D(x)\, dx = c. \tag{68}$$

The use of the equilibrium relationship (Eq. 66) to describe the monomer binding reaction (Eq. 65) implies that it is assumed that the profilin–actin binding reaction achieves a rapid equilibrium in the time scale of actin polymerization. Similar assumption has also been made for the actin filament capping reaction (Eq. 12) since equilibrium equation (Eq. 13), has been used to calculate the concentration of free filament ends, C, of Eq. 14. These are probably oversimplified schemes for interactions of actin and its regulatory proteins. At this time, very little is known about the regulating kinetics and further improvements need more biochemical information.

The hypothesis that the chemical free energy liberation of actin polymerization can be partially converted into mechanical work is a key postulate of the present model. Because of its importance, a closer look at various contributions to the free energy change during actin polymerization is provided as follows: $\Delta\mu = (\mu_G - \mu_F - \mu_P)$ is a difference of chemical potentials, in which μ_G is the chemical potential of monomeric actin·ATP in the solution, μ_F, that of polymeric actin·ADP protomer in the filament network, and μ_P, that of phosphate. For monomeric actin·ADP, $\mu_G = \mu_G^0 + k_B T \ln (c/c^0)$, in which μ_G^0 is the free energy of monomeric actin·ATP in the solution of reference concentration c^0 (say the critical concentration of polymerization), k_B is the Boltzmann constant, and T, the absolute temperature. The contribution of phosphate, μ_P, comes from hydrolysis of ATP and has a similar dependence on concentration (of phosphate) and temperature as μ_G does. For polymeric actin·ADP, $\mu_F = \mu_F^0 - lF - (F^2/2\epsilon)$, in which μ_F^0 is the free energy of actin·ADP protomer in a polymer when the filament is free of loading, F is the force exerting on the filament (negative for compression), and ϵ is the elastic coefficient of the filament assuming that it obeys Hooke's law (Hill, 1981; Hill and Kirschner, 1982). The physical significance of these expressions is that the chemical energy liberated from transition of state of one molecule from actin·ATP monomer in solution to actin·ADP protomer in a filament increases with increasing G-actin concentration in the solution and decreases with increasing compressive force exerting on the filament. The average compressive force acting on a filament barbed end is $F = (p - p_e)/n$. If one neglects the concentration effect by assuming that the concentration at the tip is almost the critical concentration (cf. Section IV), then $\Delta\mu \approx \Delta\mu^0 + (p - p_e)\, l/n + (p - p_e)^2/(2\epsilon n^2)$, where $\Delta\mu^0 = (\mu_G^0 - \mu_F^0 - \mu_P^0)$ is a constant and may be referred as a standard free energy change. Fortunately, inclusion of the details discussed here does not alter the results derived previously very much. Substituting the above expressions for $\Delta\mu$ into Eq. 7 and solving for p yield

$$p = p_e - p_a \quad \text{at} \quad x = s \tag{69a}$$

where

$$p_a = nl\epsilon\left(\frac{1+\eta}{\eta}\right)\left\{1 - \left[1 - 2\frac{\Delta\mu^0}{\epsilon l^2}\left(\frac{\eta}{1+\eta}\right)^2\right]^{1/2}\right\}. \tag{69b}$$

Thus the only modification to equations in previous sections is replacement of the equivalent active normal stress acting on the membrane applied by the filaments due to actin polymerization, $\eta\Delta\mu(n/l)$, by p_a defined by Eq. 69b.

To examine how inclusion of the effect of filament compressibility influences estimation of the efficiency of energy transduction, η is solved from Eq. 69b, which gives

$$\eta = \left(\frac{n}{l}\frac{\Delta\mu^0}{p_a} + \frac{1}{2}\frac{p_a}{nl\epsilon} - 1\right)^{-1}. \tag{70}$$

The elastic coefficient of actin filament under axial compressive loading, ϵ, can be estimated using the elastica theory from the flexural rigidity of F-actin, EI, which has been measured to be $\sim 4 \times 10^{-17}$ dyn · cm^2 (e.g., Oosawa, 1980). The derivation in the Appendix yields.

$$\epsilon = \frac{\pi^2 EI}{8h^3} = 0.4 \text{ dyn/cm}, \tag{71}$$

in which $h = 50$ nm has been used for numerical computation. This computation assumes that bending of the filaments is the primary contribution to the axial displacement of the actin filaments. The thermodynamically measured free energy liberation of actin polymerization is now understood as the standard one, $\Delta\mu^0$ ($= 4.2 \times 10^{-13}$ dyn · cm). p_a is computed from the best fit Peclet number using the definition of Pe of Eq. 25, with $\eta\Delta\mu(n/l)$ replaced by p_a. For $Pe = 0.984$ and $p_i - p_e = 0$, the equivalent active

normal stress is $p_a = 37.7$ dyn/cm^2. Using these values, the efficiency of energy transduction for pseudopod protrusion computed from Eq. 70 is 6.1×10^{-3}, essentially the same as that of Eq. 47. The relative error introduced from neglecting the compressibility of actin filaments is only 0.06% because the stresses involved here are small.

The numerical computations in Section IV show that convective mass transport of G-actin is as important as, or even dominant over, diffusive mass transport. On the other hand, for Darcy's law to be applicable to fluid flow through porous F-actin network, the convective momentum transport must be negligible compared with diffusive momentum transport. These two requirements appear to be contradictory. The answer to this paradox is simple but not trivial. The length scale used to define the mass transport Peclet number (Eq. 25) is the span of the pseudopod, whereas that controlling the fluid flow is the pore size of the F-actin network. The span of a pseudopod is orders of magnitude greater than the pore size of F-actin network. For a pseudopod of typical length of $s = 5$ μm, the length ratio of pseudopod span to F-actin network pore size is $s/h = 10^2$. For an acrosomal process of length of $s = 90$ μm, $s/h = 6 \times 10^3$. Also, the Schmidt number, Sc, which is the ratio of the molecular momentum to mass diffusivity, of the present problem is as large as $Sc = \mu/(\rho_f D) = 10^6$ (ρ_f denotes the density of fluid suspension) because the kinetic viscosity of water, $\mu/\rho_f = 10^{-2}$ cm^2/s, is several orders of magnitude greater than the diffusion coefficient, $D = 10^{-8}$ cm^2/s, of G-actin. Since the Reynolds number for fluid flow through individual pores is related to the Peclet number for transport of G-actin over the entire length of the pseudopod, by $Re = (h/s)\, Pe/Sc$, it is possible to obtain on the one hand a large mass transport Peclet number, which represents a convection-dominant mass transport, and on the other hand a small Reynolds number, which assures that the motion of the fluid can be described by Darcy's law.

It is noted that in Eq. 38 the large t asymptotic expansion of the leading term, and also in Figs. 5 and 6 the first two terms, of the large Pe perturbation series Eqs. 35–37, of the solution to Eqs. 28 are used in justifying the validity of the long-term solution (Eqs. 41) instead of the (unavailable) exact solution itself. A question arises as to how accurate the asymptotic approximations thenselves are. To exmaine this, curve of λ versus Pe are plotted in Fig. 9, *a* and *b*, using parameter values of C_1 and C_2 given by Eqs. 44 and 50, respectively, of both the exact long-term solution (the third equation of 41) and its one- and two-term asymptotic approximations (cf. the first equation of 42):

$$\lambda \approx \left(\frac{1}{2}\frac{1+C_1}{1+C_2}Pe\right)^{1/2},$$

$$\lambda \approx \left(\frac{1}{2}\frac{1+C_1}{1+C_2}Pe\right)^{1/2}\left[1+\frac{1}{2Pe(C_2-C_1)}\right]. \quad \text{as } Pe \to \infty. \tag{72}$$

After $Pe > 10$, the two curves of the exact long-term solution and its two-term asymptotic approximation in both Fig. 9, *a* and *b* become undistinguishable. The magnitude of the differences between the two curves in each pair is less than the thickness of the curves. In the case of pseudopod protrusion in leukocytes (Fig. 9 *a*), the relative error between the exact long-term solution and its two-term asymptotic approximation is <3.5% when $Pe \geq 1$. In Figs. 5, 6, and 7 *b* the validity of the long-term

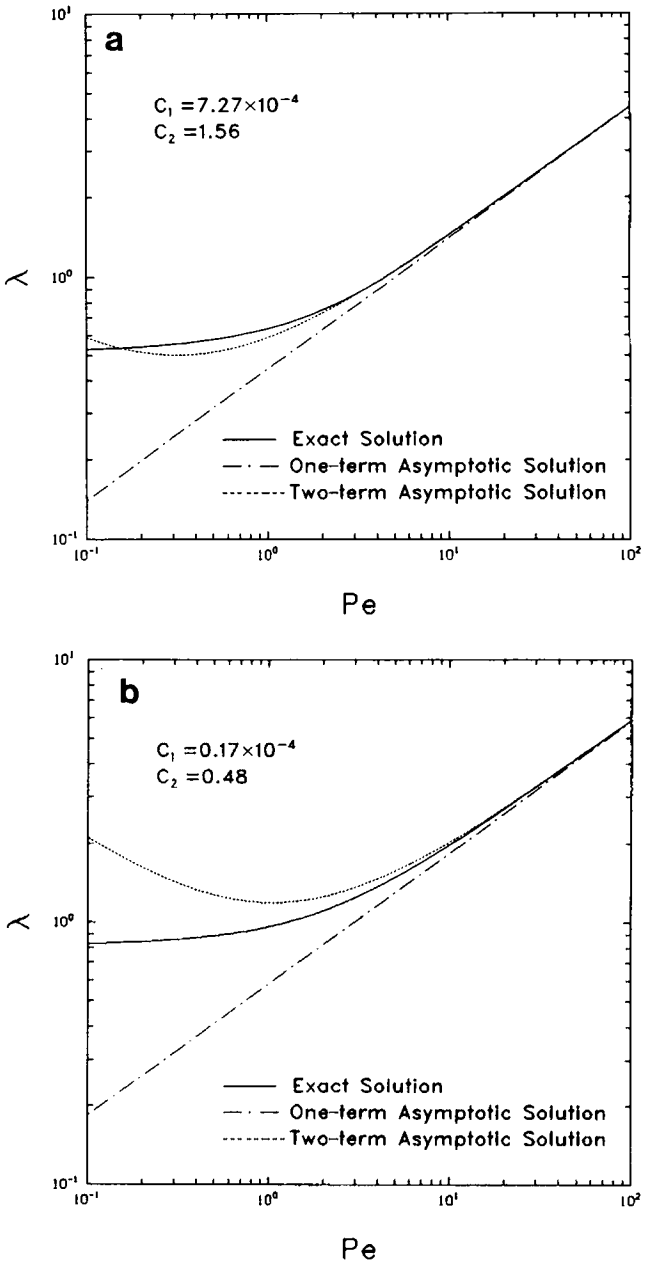

FIGURE 9 Comparison of the exact long-term solution, the third equation of 41, and its one- and two-term asymptotic approximations, Eqs. 72. *Solid curves*, exact long-term solution. *Broken lines*, one-term asymptotic approximation. *Dashed curves*, two-term asymptotic approximation. Parameters are, respectively, (*a*) $C_1 = 7.27 \times 10^{-4}$, $C_2 = 1.56$, and (*b*) $C_1 = 1.65 \times 10^{-5}$, $C_2 = 0.479$.

solution is also illustrated numerically by comparison with the perturbation solutions.

The above results do not prove that the large *Pe* perturbation solutions (Eqs. 35–37) are accurate approximations to the exact solution to Eqs. 28, nor do they prove that the long-term solution (Eqs. 41) is an accurate approximation to the exact solution (for large *Pe* cases only) but they suggest that the soltuions are consistent. There are still questions for the small *Pe* cases in which no perturbation solution is available to compare with the long-term solution. However, as demonstrated in Figs. 5 *a*, 6 *a*, and 9 *a*, and discussed in Section IV, the perturbation solution is accurate even when *Pe* is slightly smaller than unity. To summarize, the long-term approximate solution (Eqs. 41) is expected to be accurate for practical problems of time scale over one second; and the two-term asymptotic solution (Eqs. 35–37) is approximate for growth not dominated by diffusion ($Pe \geq 1$).

Comparison of the Present Model with Previous Works

Some aspects in the present model are similar to those used by other authors. Two models for elongation of acrosomal process in *Thyone* sperms which involve G-actin diffusing to, and polymerizing at, the tip of the projection have been published (Tilney and Kallenbach, 1979; Perelson and Coutsias, 1986). The first model was initially proposed by Tilney and Kallenback (1979) and later improved by Perelson and Coutsias (1986). The solution they obtained was the same as Eqs. 43 except that Tilney and Kallenbach interpreted the mass transfer Stefan number, $St = 1/C_2$, as $(c_i k_+/k_-)$ and Perelson and Coutsias, as $(c_i l/n)$. Tilney and Kallenbach did not include the conversion of G-actin into F-actin in considering the conservation of actin molecules in the polymerization zone (missing n/l term on the right-hand side of Eq. 3. The small but nonzero critical concentration of actin polymerization, (k_-/k_+), was neglected in Perelson and Coutsias' equation. So was the porous effect of the actin gel. Since both the pool concentration of the G-actin reservoir, c_i, and the concentration of filament growing points, (n/l), are orders of magnitude greater than the critical concentration, (k_-/k_+), and the porosity of F-actin network is close to one, the value of Stefan number used by Perelson and Coutsias was close to that of the present model. Thus Perelson and Coutsias' "irreversible polymerization model" is the long-term and diffusion-dominant limit of the present model.

The main differences between the second, "reversible polymerization," model of Perelson and Coutsias' and the present work are the following. The mechanical work done by actin polymerization has been postulated as the driving energy in the present model but was not considered in that of Perelson and Coutsias'. The fluid flow is governed by Darcy's law in our model whereas in model of Perelson and Coutsias' the fluid velocity was assumed to be the acrosomal growth rate, without considering the dynamics of fluid filtration. Their assumption of $v = \mathrm{d}s/\mathrm{d}t$ is not true unless $\phi = 1$ (i.e., the actin filament network has a zero volume fraction), which is actually ~0.82. When $\phi < 1$, v must be greater than $\mathrm{d}s/\mathrm{d}t$ from the consideration of mass conservation. It follows that when applying coordinate transformation (Eq. 29), Perelson and Coutsias' model led to a pure diffusion equation whereas Eqs. 30 of the present model have a nonvanishing convection term with a relative fluid velocity of $(\mathrm{d}/\mathrm{d}t)(s/Pe^{1/2}) - (Pe^{1/2}/s)$ (cf. Eqs. 30). The end-blocking effect of capping proteins has been taken into account in the present model but was not considerd in that of Perelson and Coutsias'. Thus instead of Eqs. 3 and 11 the following equations were used by Perelson and Coutsias':

$$-D\frac{\partial c}{\partial x}\bigg]_{x=s} = \frac{n}{l}\frac{\mathrm{d}s}{\mathrm{d}t} = n(k_+c - k_-)\bigg]_{x=s}. \qquad (73)$$

Based on their analysis, Perelson and Coutsias (1986) concluded that diffusion-limited actin polymerization was too slow to account for the rapid elongation of *Thyone* acrosomal process. In contrast, it has been shown in the present work that once the work done by actin polymerization is taken into account as an energy source to drive the filtration of the fluid, convection comes into play, and when convection is sufficiently strong, G-actin transport will be able to bring enough G-actin from the base to the tip of the acrosomal process to account for the rapid growth.

Oster et al. (1982) proposed a different model for elongation of acrosomal process in *Thyone* sperms based on osmotic pressure driving mechanisms due to swelling of the actin gel (see also Oster and Perelson, 1987). Their solution is also able to match the experimental data of Tilney and Inoué (1982) by adjusting free parameters. Osmotic effect may play a role at the polymerization pool at the tip of the pseudopod or acrosomal process and may provide a possible mechanical mechanism for the force generation. However, this detailed consideration has not been taken into account in the present model.

Remarks on Error Analysis

One question that arises in the data fitting concerns the values of the efficiency of transduction of chemical potential to mechanical work in actin polymerization, η. This η is orders of magnitude different in the two cases, namely, $\eta = 0.00061$ for pseudopod protrusion in leukocytes and $\eta = 0.75$ for acrosomal elongation in *Thyone* sperms. η must depend on the rate of actin polymerization as well as environmental conditions under which the reaction takes place. It is probably a function of time, and the values estimated here are only average values. Acrosomal elongation is a much faster process than pseudopod protrusion (90-μm growth in 10 s versus 6-μm growth in 30 s). This large difference in growth rates may be related to the difference in η values. Actin filaments are arranged as parallel arrays in acrosome, whereas in pseudopod they

form isotropic network. Therefore the three-dimensional effects probably play a much more important role in a pseudopod than in an acrosome. A possible explanation for the difference in η values is the regulation of actin polymerization. For example, in sperm cells there is a discrete structure, the actomere, which serves as a nucleation center for polymerization, determines the actin polarity, and guides the growing filaments into bundles. Therefore once the growth of acrosomal process starts, it may be free running. Whereas in leukocytes actin polymerization in the pseudopod may be under strict control by regulatory proteins, which slow down the polymerization process and make energy requirements very small as is reflected by a very low efficiency.

Of the many parameters that are needed in the computations, some are available in the literature while others are not. Those that are not directly available have to be calculated using the appropriate theories. Of those which are directly measured in observations some involve different (in vitro) experimental conditions, different cell types, etc. Considering the limitations on accuracy of the data, the agreement between our theory and experiments on pseudopod and acrosomal growth is regarded as satisfactory.

CONCLUSION

The notion that actin polymerization per se may be directly responsible for some kind of active cell movement is not new. It has been suggested by a number of authors and supported by some experimental evidences (Tilney, 1975; Felder, 1984). The thermodynamics aspects of which assembly and/or disassembly of actin filaments allow for the possibility of doing mechanical work has been discussed (Hill, 1981; Hill and Kirschner, 1982). However, the kinetics as to how work done by actin polymerization creates motion has not been previously elucidated. In this paper the chemical free energy liberation of actin polymerization and its conversion into mechanical work is formulated on a continuum basis. This allows the formulation of a moving boundary problem which governs the growth of the pseudopod and the motion of the fluid within the pseudopod.

The present model is intended to demonstrate the mechanism rather than to emphasize data fitting. The biological systems are more complicated than the present relatively simple model. Many of the important issues of pseudopod protrusion process have not been addressed in this model, most notably, the initiation and control mechanisms. The focus here is on the mechanical aspects, and the results show that the basic hypotheses are possible.

To summarize, this work utilizes the observed morphology of human leukocytes, the biochemical knowledge of actin polymerization, and the theory of continuum mechanics to model the pseudopod protrusion process in leukocytes. The proposed model links together observations in various experimental studies and provides a unified theoretical scheme consistent with the known data. It shows that apparently different phenomena, such as protrusion of pseudopod in leukocytes and elongation of acrosomal process in sperms, can be explained by different parameters but similar mechanisms.

APPENDIX

Esimation of the Compressive Elastic Coefficient of F-actin

The inclusion of compressibility of F-actin in the calculation of the chemical potential of an actin protomer in a polymer requires information about the compressive elastic coefficient of F-actin, which is unavailable in the literature. In this appendix an estimation of this coefficient, ϵ, is presented based on the theory of large deflections of buckled bars (the elastica).

As illustrated schematically in Fig. 10, when a long, slender cantilever beam (of length h and flexural rigidity EI) like an actin filament under axial compressive load F (negative for compression) on its free end, the major contribution to the axial displacement, u (along the undeformed configuration, positive in positive x direction), comes from buckling and that from compresssion is negligible. The following solution has been obtained from the theory of the elastica (cf. Timoshenko and Gere, 1961, pp. 76–82).

$$h = \sqrt{\frac{EI}{-F}}\,K\left(\sin\frac{\theta}{2}\right),$$

$$u = 2\sqrt{\frac{EI}{-F}}\,E\left(\sin\frac{\theta}{2}\right) - 2h, \tag{74}$$

where θ is the angle of rotation at the tip, $K(\cdot)$ and $E(\cdot)$ are, respectively, the complete elliptic integrals of the first and the second kinds (Abramowitz and Stegun, 1964). Elimination of $\sin(\theta/2)$ in the above equations leads to

$$u = 2\sqrt{\frac{EI}{-F}}\,E\left[K^{-1}\left(h\sqrt{\frac{-F}{EI}}\right)\right] - 2h, \tag{75}$$

in which $K(\cdot)^{-1}$ denotes the inverse function of $K(\cdot)$. Eq. 75 gives the axial displacement u as a function of the compressive force F. Its inverse gives the nonlinear elastic law for the compressive F-actin. The compressive elastic constant is the coefficient of the linear term in the Taylor series expansion of the nonlinear elastic law, i.e.,

$$\epsilon = \left.\frac{dF}{du}\right|_{u=0} = 1\Big/\left.\frac{du}{dF}\right|_{F=0} = \frac{\pi^2}{8}\frac{EI}{h^3},$$

which is the same as Eq. 71 in text.

The authors thank Dr. G. W. Schmid-Schönbein for many discussions and providing us with experimental data. We also thank Drs. T. P.

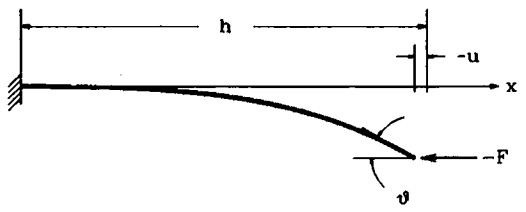

FIGURE 10 Large deflection of a buckled cantilever beam.

Stossel, K. S. Zaner, Y.-L. Wang, K.-L. P., and L. A. Sung, V. Prasad, M. B. Friedman, and Ms. R. Y. Tsai for helpful discussions.

This work was supported by National Institutes of Health grant No. HL-16851.

Received for publication 24 March 1988 and in final form 8 August 1988.

REFERENCES

Abramowitz, M., and I. A. Stegun. 1964. Handbook of Mathematical Functions. National Bureau of Standards, Washington, D.C.

Aebi, U., W. E. Fowler, G. Isenberg, T. D. Pollard, and P. R. Smith. 1981. Crystalline actin sheets: their structure and polymorphism. *J. Cell Biol.* 91:340–351.

Carson, M., A. Weber, and S. H. Zigmond. 1986. An actin-nucleating activity in polymorphonuclear leukocytes is modulated by chemotactic peptides. *J. Cell Biol.* 130:2707–2714.

Chien, S., K.-L. P. Sung, R. Skalak, and G. W. Schmid-Schönbein. 1982. Viscoelastic properties of leukocytes in passive deformation. *In* White Blood Cells: Morphology and Rheology as Realted to Function. U. Bagge, G. V. R. Born, and P. Gaehtgens, editors. Martinus Nijhoff Publishers, The Hague-Boston-London. 11–20.

Chein, S., G. W. Schmid-Schönbein, K.-L. P. Sung, E. A. Schmalzer, and R. Skalak. 1984. Viscoelastic properties of leukocytes. *In* White Cell Mechanics: Basic Science and Clinical Aspects. H. J. Meiselman, M. A. Lichtman, and P. L. LaCelle, editors. Alan R, Liss Inc., New York, 19–51.

Cooper, J. A., J. D. Blum, and T. D. Pollard. 1984. *Acanthamoeba castellanii* capping protein: properties, mechanism of action, immunologic cross-reactivity, and localization. *J. Cell Biol.* 99:217–225.

Crank, J. 1984. Free and Moving Boundary Problems. Clarendon Press, Oxford.

Curry, F.-R. E. 1986. Determinants of capillary permeability: a review of mechanisms based on single capillary studies in the frog. *Circ. Res.* 39:367–380.

Dembo, M. 1986. The mechanics of motility in dissociated cytoplasm. *Biophys. J.* 50:1165–1183.

Dembo, M., and F. Harlow. 1986. Cell motion, contractile network, and the physics of interpenetrating reactive flow. *Biophys. J.* 50:109–121.

Dembo, M., F. Harlow, and W. Alt. 1984. The biophysics of cell motility. *In* Cell Surface Dynamics: Concepts and Models. A. S. Perelson, C. DeLisi, and F. W. Wiegel, editors. Marcel Dekker, New York, 495–541.

Detmers, P. A., U. W. Goodenough, and J. Condeelis. 1983. Elongation of the fertilization tubule in *Chlamydomonas:* new observations on the core microfilaments and the effect of transient intracellular signals on their structural integrity. *J. Cell Biol.* 97:522–532.

Dong, C., R. Skalak, K.-L. P. Sung, G. W. Schmid-Schönbein, and S. Chien. 1988. Passive deformation analysis of human leukocytes. *J. Biomech. Eng.* 110:27–36.

Felder, S. 1984. Mechanics and Molecular Dynamics of Fibroblast Locomotion. Ph. D. Dissertation, Department of Biological Chemistry, Washington University, St. Louis, Missouri.

Frieden, C. 1985. Actin and tubulin polymerization: the use of kinetic methods to determine mechanism. *Annu. Rev. Biophys. Chem.* 14:189–210.

Gershon, N. D., K. P. Porter, and B. L. Trus. 1985. The cytoplasmic matrix: its volume and surface area and the diffusion of molecules through it. *Proc. Natl. Acad. Sci. USA.* 82:5030–5034.

Glenney, J. R., P. Kaulfus Jr., and K. Weber. 1981. F actin assembly modulated by villin: Ca^{++}-dependent nucleation and capping of the barbed end. *Cell.* 24:471–480.

Gordon, D. J., Y.-Z. Yang, and E. D. Korn. 1976. Polymerization of *Acanthamoeba* actin: kinetics, thermodynamics, and co-polymerization with muscle actin. *J. Biol. Chem.* 251:7474–7479.

Happel, J., and H. Brenner, 1973. Low Reynolds Number Hydrodynamics. 2nd ed. Martinus Nijhoff Publishers, Dordrecht-Boston-Lancaster.

Hartwig, J. H., and P. Shevlin. 1986. The architecture of actin filaments and the ultrastructural location of actin-binding protein in the periphery of lung macrophages. *J. Cell Biol.* 103:1007–1020.

Hill, T. L. 1981. Microfilament or microtubule assembly or disassembly against a force. *Proc. Natl. Acad. Sci. USA.* 78:5613–5617.

Hill, T. L., and M. W. Kirschner. 1982. Subunit Treadmilling of microtubules of actin in the presence of cellular barriers: possible conversion of chemical free energy into mechanical work. *Proc. Natl. Acad. Sci. USA.* 79:480–484.

Jacobson, K., and J. Wojcieszyn. 1984. The translation mobility of substances within the cytoplasmic matrix. *Proc. Natl. Acad. Sci. USA.* 81:6747–6751.

Janmey, P. A., C. Chaponnier, S. E. Lind, K. S. Zaner, T. P. Stossel, and H. L. Yin. 1985. Interactions of gelsolin and gelsolin-actin complexes with actin. Effects of calcium on actin nucleation, filament severing, and end blocking. *Biochemistry.* 24:3714–3723.

Korn, E. D. 1982. Actin polymerization and its regulation by proteins from nonmuscle cells. *Physiol. Rev.* 62:672–737.

Kreis, T. E., B. Geiger, and J. Schlessinger. 1982. Mobility of microinjected rhodamine actin within living chicken gizzard cells determined by fluorescence photobleaching recovery. *Cell.* 29:835–845.

Lal, A. A., and E. D. Korn. 1985. Reinvestigation of the inhibition of actin polymerization by profilin. *J. Biol. Chem.* 260:10132–10138.

Lanir, Y. 1987*a*. Biorheology and fluid flux in swelling tissues. I. Bicomponent theory for small deformations, including concentration effects. *Biorheol.* 24:173–187.

Lanir, Y. 1987*b*. Biorheology and fluid flux in swelling tissues. II. Analysis of unconfined compressive response of transversely isotropic cartilage disc. *Biorheol.* 24:189–205.

Lanni, F., and B. R. Ware. 1984. Detection and characterization of actin monomers, oligomers, and filaments in solution by measurement of fluorescence photobleaching recovery. *Biophys. J.* 46:97–110.

Lanni, F., D. L. Taylor, and B. R. Ware. 1981. Fluorescence photobleaching recovery in solutions of labeled actin. *Biophys. J.* 35:351–364.

Lassing, I., and U. Lindberg. 1985. Specific interaction between phosphatidylinositol 4, 5-bisphosphate and profilin. *Nature (Lond.).* 314:472–474.

Luby-Phelps, K., D. L. Taylor, and F. Lanni. 1986. Probing the structure of cytoplasm. *J. Cell Biol.* 102:2015–2022.

Mihashi, K. 1964. Molecular characteristics of G-ADP actin. *Arch. Biochem. Biophys.* 107:441–448.

Montague, C., K. W. Rhee, and F. D. Carlson. 1983. Measurement of the translational diffusion constant of G-actin by photon correlation spectroscopy. *J. Musc. Res. Cell Motil.* 4:95–101.

Nayfeh, A. H. 1981. Introduction to Perturbation Techniques. John Wiley & Sons, Inc., New York.

Nossal, R. 1988. On the elasticity of cytoskeletal networks. *Biophys. J.* 53:349–359.

Oosawa, F. 1980. The flexibility of F-actin. *Biophys. Chem.* 11:443–446.

Orenstein, J. M., and E. Shelton. 1977. Membrane phenomena accompanying erythrophagocytosis. A scanning electron microscopy study. *Lab. Invest.* 36:363–374.

Oster, G. F. 1984. On the crawling of cells. *J. Embryol. Exp. Morphol.* 83 (Suppl.):329–364.

Oster, G. F., and G. M. Odell. 1984. The mechanochemistry of cytogels. *Physica.* 12D:333–350.

Oster, G. F., and A. S. Perelson. 1985. Cell spreading and motility: a model lamellipod. *J. Math. Biol.* 21:383–388.

Oster, G. F., and A. S. Perelson. 1987. The physics of cell motility. *J. Cell Sci.* 8:35–54.

Oster, G. F., A. S. Perelson, and L. G. Tilney. 1982. A mechanical model for elongation of the acrosomal process in *Thyone* sperm. *J. Math. Biol.* 15:259–265.

Perelson, A. S., and E. A. Coutsias. 1986. A moving boundary model of acrosomal elongation. *J. Math. Biol.* 23:361–378.

Pollard, T. D. 1986. Rate constants for the reactions of ATP- and ADP-actin with the ends of actin filaments. *J. Cell Biol.* 103:2747–2754.

Pollard, T.D., and J. A. Cooper. 1984. Quantitative analysis of the effect of *Acanthamoeba* profilin on actin filament nucleation and elongation. *Biochemistry.* 23:6631–6641.

Pollard, T. D., and J. A. Cooper. 1986. Actin and actin-binding proteins. A critical evaluation of mechansims and functions. *Annu. Rev. Biochem.* 55:987–1035.

Pollard, T. D., and M. S. Mooseker. 1981. Direct measurement of actin polymerization rate constants by electron microscopy of actin filaments nucleated by isolated microvillus cores. *J. Cell Biol.* 88:654–659.

Pryzwansky, K. B., M. Schliwa, and K. R. Porter. 1983. Comparison of the three-dimensional organization of unextracted and Triton-extracted human neutrophilic polymorphonuclear leukocytes. *Eur. J. Cell Biol.* 30:112–125.

Scheidegger, A. E. 1974. The Physics of Flow through Porous Media. 3rd ed. University of Toronto Press, Toronto-Buffalo.

Schmid-Schönbein, G. W. 1987. Rheology of leukocytes. *In* Handbook of Bioengineering. R. Skalak, and S. Chien, editors. McGraw Hill, New York. 13.1–13.25

Schmid-Schönbein, G. W., and R. Skalak. 1984. Continuum mechanical model of leukocytes during protopod formation. *J. Biomech. Eng.* 106:10–18.

Schmid-Schönbein, G. W., K.-L. P. Sung, H. Tözeren, R. Skalak, and S. Chien. 1981. Passive mechanical properties of human leukocytes. *Biophys. J.* 36:243–256.

Schmid-Schönbein, G. W., R. Skalak, K.-L. P. Sung, and S. Chien. 1982. Human leukocytes in the active state. *In* White Blood Cells: Morphology and Rheology as Related to Function. U. Bagge, G. V. R. Born, and P. Gaehtgens, editors. Martinus Nijhoff Publishers, The Hague-Boston-London. 21–31.

Stossel, T. P. 1988. Leukocytes: mechanical responses. *In* Inflammation: Basic Principles and Clinical Correlates. J. I. Gallin, I. M. Goldstein, and P. Snyderman, editors. Raven Press, New York, 325–342.

Stossel, T. P., J. H. Hartwig, H. L. Yin, and O. Stendahl. 1981. The motor of amoeboid leukocytes. *Biochem. Soc. Symp.* 45:51–63.

Sung, K.-L. P., G. W. Schmid-Schönbein, R. Skalak, G. B. Schuessler, S. Usami, and S. Chien. 1982. Influence of physiochemical factors on rheology of human neutrophils. *Biophys. J.* 39:101–106.

Tait, J. F., and C. Frieden. 1982. Polymerization and gelation of actin studied by fluorescence photobleaching recovery. *Biochemistry.* 21:3666–3674.

Tilney, L. G. 1975. The role of actin in nonmuscle cell motility. *In* Molecules and Cell Movement. S. Inoué and R. E. Stephens, editors. Raven Press, New York. 339–386.

Tilney, L. G., and S. Inoué. 1982. Acrosomal reaction of *Thyone* sperm. II. The kinetics and possible mechansim of acrosomal process elongation. *J. Cell Biol.* 93:820–827.

Tilney, L. G., and N. Kallenbach. 1979. Polymerization of actin. VI. The polarity of the actin filaments in the acrosomal process and how it might be determined. *J. Cell Biol.* 81:608–623.

Tilney, L. G., E. M. Bonder, and D J. DeRosier. 1981. Actin filaments elongate from their membrane-associated ends. *J. Cell Biol.* 90:485–494.

Timoshenko, S. P., and J. M. Gere. 1961. Theory of Elastic Stability. 2nd ed. McGraw-Hill, New York-Toronto-London.

Tobacman, L. S., and E. D. Korn. 1982. The regulation of actin polymerization and the inhibition of monomeric actin ATPase activity by *Acanthamoeba* profilin. *J. Biol. Chem.* 257:4166–4170.

Tranquillo, R. T., and D. A. Lauffenburger. 1987. Stochastic model of leukocyte chemosensory movement. *J. Math. Biol.* 25:229–262.

Tranquillo, R. T., D. A. Lauffenburger, and S. H. Zigmond. 1988. A stochastic model for leukocyte random motility and chemotaxis based on receptor binding fluctuations. *J. Cell Biol.* 106:303–309.

Walsh, T. P., A. Weber, J. Higgins, E. M. Bonder, and M. S. Mooseker. 1984. Effect of villin on the kinetics of actin polymerization. *Biochemistry.* 23:2613–2621.

Wang, Y.-L. 1985. Exchange of actin subunits at the leading edge of living fibroblasts: possible role of treadmilling. *J. Cell Biol.* 101:597–602.

Wang, Y.-L., F. Lanni, P. L. McNeil, B. R. Ware, and D. L. Taylor. 1982. Mobility of cytoplasmic and membrane-associated actin in living cells. *Proc. Natl. Acad. Sci. USA.* 79:4660–4664.

Wanger, M., and A. Wegner. 1985. Equilibrium constant for binding of an actin filament capping protein to the barbed end of actin filaments. *Biochemistry.* 24:1035–1040.

Wenger, A., and P. Savko. 1982. Fragmentation of actin filaments. *Biochemistry.* 21:1909–1913.

Yin, H. L., J. H. Albrecht, and A. Fattoum. 1981. Identification of gelsolin, a Ca^{2+}-dependent regulatory protein of actin gel-sol transformation, and its intracellular distribution in a variety of cells and tissues. *J. Cell Biol.* 91:901–904.